Madden–Julian Oscillation: Its Discovery, Dynamics, and Impact on East Asia

Tim LI[1,2*], Jian LING[3], and Pang-Chi HSU[1]

1 *Key Laboratory of Meteorological Disaster, Ministry of Education (KLME)/Joint International Research Laboratory of Climate and Environmental Change (ILCEC)/Collaborative Innovation Center on Forecast and Evaluation of Meteorological Disasters (CIC-FEMD), Nanjing University of Information Science &Technology, Nanjing* 210044, *China*

2 *International Pacific Research Center and Department of Atmospheric Sciences, School of Ocean and Earth Science and Technology, University of Hawaii at Manoa, Honolulu, HI* 96822, *USA*

3 *State Key Laboratory of Numerical Modeling for Atmospheric Sciences and Geophysical Fluid Dynamics, Institute of Atmospheric Physics, Chinese Academy of Sciences, Beijing* 100029, *China*

(Received September 9, 2019; in final form December 20, 2019)

ABSTRACT

In this review article, we pay primary attention to innovative works in the Madden–Julian Oscillation (MJO) field done by Chinese scientists. The historical aspect of discovery of the MJO and earlier studies of its dynamics by Chinese scientists are first described. It is followed by the description of recent advances in MJO propagation and initiation dynamics. For MJO eastward propagation, two types of the moisture mode theory are introduced. The first one emphasizes the effect of zonal asymmetry of perturbation moisture in the atmospheric boundary layer and the second one emphasizes the zonal asymmetry of column integrated moisture static energy (MSE) tendency. The mechanisms for MJO initiation over the western Indian Ocean include three distinctive processes: lower tropospheric moistening due to horizontal advection caused by preceding suppressed-phase MJO, midlatitude Rossby wave activity flux convergence in the upper troposphere originated from the Southern Hemisphere, and a delayed sea surface temperature feedback in association with a preceding opposite-phase MJO. The impacts of MJO on low-frequency variability of precipitation and temperature and associated extreme events in East Asia are also discussed.

Key words: Madden–Julian Oscillation (MJO), propagation and initiation, lower tropospheric moistening, Rossby wave activity flux, delayed sea surface temperature feedback

Citation: Li, T., J. Ling, and P.-C. Hsu, 2020: Madden–Julian Oscillation: Its discovery, dynamics, and impact on East Asia. *J. Meteor. Res.*, **34**(1), 20–42, doi: 10.1007/s13351-020-9153-3.

1. Introduction

The tropical atmosphere exhibits rich spectrum of multiple temporal and spatial scales. Among them is a marked intraseasonal oscillation (ISO). This sub-seasonal scale variability was originally discovered by Madden and Julian (1971) based on the power spectrum analysis of surface pressure and low- and upper-level zonal wind fields at an island station over central equatorial Pacific. Later, Madden and Julian (1972) further illustrated that this variability appears over the large domain of the tropics and has a coherent dynamic structure, propagating slowly eastward. The originally identified ISO signal by Madden and Julian (1971, 1972) was confined in the 40–50-day period with typical zonal wavenumber one and eastward-propagating characteristics, which were confirmed by later studies using modern observational data (e.g., Krishnamurti and Subrahmanyam, 1982; Weickmann, 1983; Murakami and Nakazawa, 1985; Lau and Chan, 1986; Knutson and Weickmann, 1987; Chen and Murakami, 1988; Hartmann and Michelsen, 1989). The later studies with multiple data sources and multiple variables showed that this oscillation is of more broadband (20–90 days) than the original 40–50-day period

Supported by the National Key Research and Development Program of China (2018YFC1505804), National Natural Science Foundation of China (41875069, 41575043, 41575052, 41922035, 41520104, and 41575062), US NSF AGS-1643297, and NOAA NA18OAR4310298. This is SOEST contribution number 10900 and IPRC contribution number 1428.

*Corresponding author: timli@hawaii.edu.

(e.g., Krishnamurti and Subrahmanyam, 1982; Wang and Rui, 1990; Hendon and Salby, 1994; Sperber et al., 1997; Annamalai and Slingo, 2001; Zhang, 2005).

The ISO signals exhibit pronounced seasonality in propagation (Madden, 1986; Wang and Rui, 1990; Madden and Julian, 1994; Jones et al., 2004; Zhang and Dong, 2004; Kikuchi et al., 2012; Lu and Hsu, 2017) and initiation (Jiang and Li, 2005; Wang et al., 2006; Zhao et al., 2013; Li et al., 2015). In boreal winter, ISO is characterized by pronounced eastward propagation along the seasonal mean convective zones over tropical Indian Ocean and Maritime Continent regions (Hendon and Salby, 1994; Salby and Hendon, 1994; Hsu and Li, 2012; Zhao et al., 2013). This eastward-propagating mode is often referred to as the MJO mode. The boreal summer ISO (hereafter BSISO) is characterized by pronounced northward propagation over the tropical Indian Ocean and South China Sea (Yasunari, 1979; Jiang et al., 2004; Li et al., 2018) and northwestward propagation over western North Pacific (Li and Wang, 2005).

The distinctive propagation characteristics between boreal winter and summer are caused by the background annual cycle mean state, as demonstrated by a linear stability analysis (Li, 2014). Under a northern winter mean state in which the thermal equator shifts slightly southward within one Rossby radius of deformation, convectively coupled Kelvin waves are unstable while Rossby waves are stable. As a result, the MJO perturbation moves eastward along the mean convective zone. Under a boreal summer mean state in which the thermal equator shifts far away from one Rossby radius of deformation and there is subsidence over the equatorial region, Kelvin waves are damped while Rossby waves become unstable. This promotes the northward jump of ISO convection away from the equator.

The initiation of ISO convection is also quite different between boreal winter and summer over tropical Indian Ocean (IO). In boreal winter ISO convection often initiates over southwestern IO (Zhao et al., 2013), while in boreal summer ISO convection is often triggered over central equatorial IO (Wang et al., 2006; Zhang et al., 2019). The difference is possibly caused by the seasonal change of the mean SST over the tropical IO (Zhang et al., 2019).

MJO/ISO has been identified to have far reaching impacts on global weather and climate. For example, during its eastward propagating journey, MJO may trigger the monsoon onset (Li et al., 2013) and affect the monsoon active and break periods (Jiang et al., 2004; Qi et al., 2008; Hsu and Yang, 2016). It may help trigger the El Niño–Southern Oscillation (ENSO) events through induced westerly wind burst (Lengaigne et al., 2004; Chen et al., 2017) and interact with diurnal cycles (Lu et al., 2019) and high-frequency disturbances (Zhu et al., 2019) over Maritime Continent. The tropical IO and western North Pacific (WNP) are regions of strong ISO variability. These regions, not by coincidence, are also regions with most active synoptic-scale variability (SSV) including synoptic wave train and TC activity (Lau and Lau, 1990; Liebmann et al., 1994; Hartmann and Maloney, 2001; Maloney and Dickinson, 2003; Straub and Kiladis, 2003; Batstone et al., 2005). It is well known that ISO exerts a large-scale control on SSV (Hendon and Liebmann, 1994; Maloney and Hartmann, 1998, 2000a, b; Straub and Kiladis, 2003). SSV, on the other hand, may exert an upscale feedback to MJO through nonlinear rectification of diabatic heating (Hsu and Li, 2011; Zhu et al., 2019) and surface latent heat flux (Zhou and Li, 2010), eddy momentum transport (Hsu and Li, 2011; Zhu et al., 2019), and barotropic energy conversion (Hsu et al., 2011).

MJO is the major predictability source for extended-range weather–climate forecast. Through 100-yr efforts, short-range weather forecast is now quite mature. Understanding ENSO dynamics and improved simulation of ENSO in coupled atmosphere–ocean models make it possible for seasonal prediction. Currently, the most difficult part in operational centers is extended range (10–30-day) forecast. Because of that, the World Meteorological Organization (WMO) called for grand challenging to fill in the large forecast skill gap between short-range weather and long-range seasonal prediction. Accurate prediction of MJO/ISO is crucial for bridging the gap.

Most of state-of-the-art global models, however, have low skills in simulating MJO eastward propagation (Wang et al., 2017). Our current knowledge in understanding MJO/ISO dynamics is limited. Thus, revealing the MJO fundamental dynamics including its propagation and initiation mechanisms is critical for advancing tropical climate dynamics, improving model capability in predicting intraseasonal variations of the global atmosphere and ocean, and bridging the current gap between short-range weather and seasonal climate prediction.

Different from previous MJO review literatures (Zhang, 2005; Waliser, 2006), this article pays more attention to the innovative works in the MJO field done by Chinese scientists. The objective of this paper is to review the historical aspect of MJO discovery and some earlier studies of MJO by Chinese scientists, introduce some latest advancement in understanding MJO propagation and initiation dynamics in international research community, and describe the impact of MJO on extreme

weather events in China and East Asia. The remaining part of this paper is organized as follows. In Section 2, we describe the discovery of MJO and some theoretical studies by Chinese scientists in earlier days. In particular, Xie et al. (1963) discovered a 40–50-day oscillation in the Asian monsoon region, and this paper was published in a Chinese journal eight years before Madden and Julian (1971). In Section 3, we introduce various theories for MJO eastward propagation, with an emphasis on the recently developed moisture mode theory. In addition, physical processes relevant to MJO initiation are also discussed. In Section 4, we pay special attention to MJO/ISO impacts on the East Asian climate. Finally, a summary and concluding remark are given in the last section.

2. Historical perspective of discovery and study of MJO by Chinese scientists

Madden and Julian (1971) unveiled a 40–50-day oscillation in the tropospheric zonal wind using radiosonde observation at Canton Island in the central Pacific. This oscillation was later found connected to a broad global tropical circulation based on observations from multiple stations across the tropics (Madden and Julian, 1972). The intraseasonal signal is now referred to as the Madden–Julian Oscillation (MJO). The discovery of MJO may be regarded as one of the most important discoveries on tropical atmosphere in the 20th century. Papers by Madden and Julian (1971, 1972) are among the most influential and most cited studies in modern meteorology.

One important effect of MJO is its impact on tropical cyclone (TC) genesis. Liebmann et al. (1994) indicated that the frequency of TC genesis during the active phase of MJO is twice as large as that during the inactive phase of MJO. Maloney and Hartmann (1998, 2000a, b) suggested that MJO westerlies may set up favorable environmental conditions for TC development by inducing low-level cyclonic vorticity and weak vertical wind shear. Small-scale eddies may grow through barotropic eddy kinetic energy (EKE) conversion from the MJO background mean flow, serving as the energy source for TC development (Hartmann and Maloney, 2001; Maloney and Hartmann, 2001; Hsu et al., 2011). Sensitivity model experiments showed that both MJO-scale circulation and moisture anomalies contribute to TC development (Cao et al., 2014) and such a forcing effect is basin dependent (Zhao and Li, 2019).

Li et al. (2018) published an article in *Bulletin of the American Meteorological Society* (BAMS) and informed the community that the 40–50-day oscillation was first discovered by Chinese scientists (Xie et al., 1963, abbreviated as Xie63 hereafter) in a Chinese journal "*Acta Meteorologica Sinica*," eight years before Madden and Julian's seminal work. Xie et al. (1963) documented an oscillatory signal of 40–50-day period using raw radiosonde data from several stations in the tropics extended from 70°E all the way to central Pacific. Their analysis data covered three years from 1958 to 1960 for the months of June to September. The 40–50-day signal discovered by Xie63 is strikingly strong as revealed by the total zonal wind component at 700 hPa over these stations without any filtering (Fig. 1). In addition, Xie63 also documented a relation between the low-frequency zonal wind oscillation and the occurrence of typhoons in the western Pacific. They noted that typhoons often appeared in the confluence region where the monsoon westerly meets the trade easterly.

Here is a direct quote, with its English translation, of the abstract of Xie63:

"The relationship between the basic flows of the low latitudes and the occurrence of typhoons was investigated statistically and synoptically by means of recent three-year radiosonde data. It was found that about 80% of typhoons developed in the eastern flank of the tropical confluence zone between the monsoon westerlies and the easterly trade winds. The westerlies are a large-scale and quasi-steady phenomenon. Thus it is probably reasonable to be called the "basic flow" while the typhoons are considered as vortices of smaller scale. There is a quite definite relationship between the time, location and frequency of typhoon genesis and the location and strength of the basic flow in the low latitudes. There was a quasi-periodical oscillation of strength and position of the basic zonal flow with a period longer than one month. Such an oscillation might be helpful for the extended-range forecast of initiation and development of typhoons."

Irrespective of the importance of these findings more than 50 years ago, the original paper by Xie63 was published in Chinese and remains mostly unknown to the international research community. Li et al. (2018) brought attention of the study by Xie63 and its originality to MJO community worldwide. Using modern satellite and reanalysis data, Li et al. (2018) verified the results of Xie63 and compared the results of Xie63 and Madden and Julian (1971) using a longer period of data (1958–1970), to have a better comparison of ISO signals found by Xie63 and Madden and Julian (1971). In addition, the origin of the oscillation in the monsoon westerly was discussed and its relationship with the occurrence of TCs was confirmed.

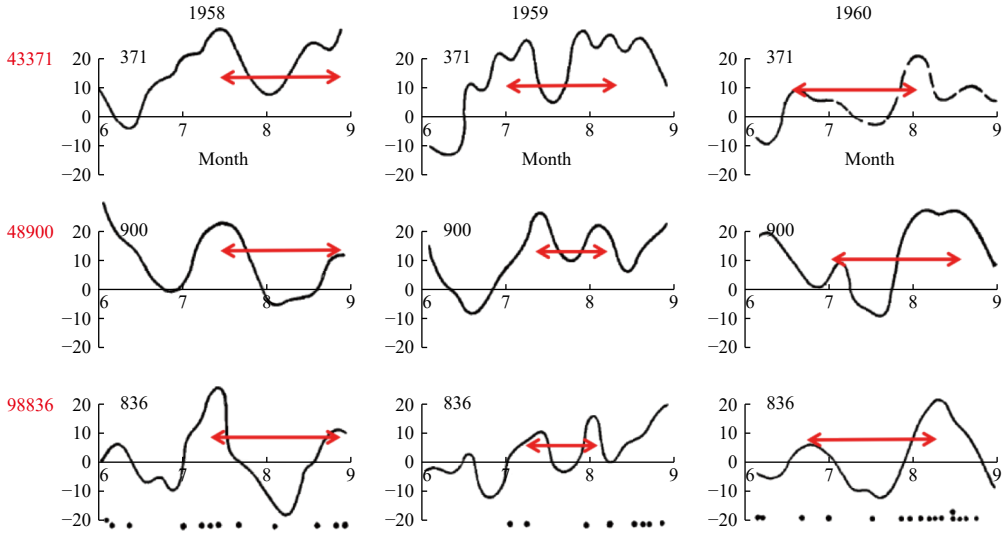

Fig. 1. Original Fig. 2 from Xie63 showing time series of 5-day running-mean zonal wind (m s^{-1}) at 700 hPa. Positive (negative) values indicate westerly (easterly). The abscissa represents time from 1 June to 1 September. The station number is marked in red to the left of each row of panels and the first column is for 1958, the second for 1959, and the third for 1960. Black dots at the bottom denote the occurrence of typhoons each year. Red arrows are added by the authors of the current study to highlight the intraseasonal periods.

Following Xie et al. (1963), Ding et al. (1977) published a paper in Chinese to investigate how the confluent low-frequency mean flow might modulate multiple TC formation. They found that multiple TC formation events often happened in the region where there was strong interaction between northern and southern hemispheric circulation. Such environmental flows favor the development of multiple tropical cyclones through the Conditional Instability of Second Kind (CISK).

Li (1983) explored the relationships of the tropical wave instability and the vertical profiles of convective heating using a linear atmospheric model in an axisymmetric cylinder coordinate system. He found that the growth rate of the oscillatory unstable modes only occurred at large horizontal scales (4,500 km), and the preferred horizontal scale is the largest when maximum heating appeared in the lower troposphere. The result suggested that the vertical structure of convective heating is an important factor for large-scale atmospheric disturbances. The sensitivity to the vertical distribution of the diabatic heating was further investigated by using a general circulation model (Li et al., 2009). No systematic eastward propagation over the Indian and western Pacific Oceans was reproduced when the heating profile was top heavy. Eastward propagating perturbations were simulated with a phase speed similar to that of the MJO only when the diabatic heating was set to bottom heavy (Li et al., 2009). MJO instability mechanism was investigated by Li (1985), who considered the cumulus convective heating feedback, following the idea of CISK. This feedback mechanism was suggested to play an important role in the initiation and maintenance of MJO in the tropics. Lau and Peng (1987) expanded this theory into a mobile wave CISK theory that could better explain the slow eastward propagation of MJO. Li et al. (2002) further studied the mechanism of MJO propagation using an air–sea coupled model including both the CISK and evaporation–wind feedback mechanisms, and found that the CISK mechanism played a critical role in the MJO dynamics.

3. Recent advances in understanding MJO propagation and initiation dynamics

In this section, we will review the physical mechanisms relevant to MJO eastward propagation and initiation, with an emphasis on latest development in the recent decade. The most striking feature of MJO is its slow eastward phase propagation along equatorial Indian Ocean and western Pacific after being triggered over the western Indian Ocean (Madden and Julian, 1972; Zhao et al., 2013). The anomalous circulation associated with MJO has a zonal wavenumber-1 structure with a Kelvin wave type circulation to the east and a Rossby wave gyre circulation to the west (Hendon and Salby, 1994; Wang and Li, 1994; Li and Zhou, 2009). Vertically it has a first-baroclinic mode structure in the free atmosphere and a phase lead of moisture and convergence anomalies in the planetary boundary layer (PBL), relative to the MJO convection (Wang and Rui, 1990; Sperber, 2003; Hsu and Li, 2012). Compared to the MJO, the BSISO exhibits a more complicated propagating characteristic with

pronounced northward propagation over northern Indian Ocean and South China Sea and northwestward propagation over western North Pacific (e.g., Yasunari, 1979; Lau and Chan, 1986; Wang and Rui, 1990; Hsu and Weng, 2001; Lawrence and Webster, 2002; Jiang et al., 2004; Li and Wang, 2005; Tsou et al., 2005).

3.1 *Mechanism for MJO eastward propagation*

Various theories have been proposed to understand MJO eastward phase propagation. Early studies assumed that the oscillation is a Kelvin wave forced by convective heating through a so called wave–CISK mechanism (Lau and Peng, 1987; Chang and Lim, 1988; Wang, 1988a). The major promise of this mechanism is that heating effect can be represented by wave induced moisture convergence so that its net effect is the reduction of atmospheric static stability and thus the slowing-down of atmospheric Kelvin waves in the tropics. The weakness of this mechanism is that it prefers maximum growth in small scale, which is against the observation.

The second theory is the Wind-Induced Surface Heat Exchange (WISHE) feedback (Emanuel, 1987; Neelin et al., 1987), which assumes a conditionally unstable atmosphere so that surface heat flux anomaly may trigger atmospheric heating to the east of MJO main convection under the equatorial mean easterly. However, in reality, the observed mean flow over the Indo-Pacific warm pool is dominated by westerly flow. As a result, this mechanism favors a westward rather than an eastward phase propagation (Wang, 1988b; Wang et al., 2017).

The third theory emphasized the role of a PBL frictional effect (Wang, 1988a; Wang and Li, 1994). A PBL convergence anomaly appears to the east of MJO main convection, which causes the column integrated moisture convergence center shifting slightly to the east of the MJO center, results in eastward moving tendency (Li and Wang, 1994; Wang and Li, 1994). But such a heating tendency depends on model convective parameterization. Idealized numerical experiments with an aqua-planet atmospheric GCM show that there is no clear eastward propagation when perturbation moisture asymmetry is removed even though PBL convergence asymmetry is still presented (Hsu et al., 2014).

Recently, two distinctive moisture mode theories were proposed. Both of the theories emphasize the important role of MJO-scale moisture anomaly in its eastward propagation. The first moisture mode theory emphasizes the role of zonal asymmetry of perturbation moisture in the atmospheric PBL (Hsu and Li, 2012). The other moisture mode theory stresses the importance of zonal asymmetry of time tendency of column integrated moist static energy (MSE) anomaly, regardless of whether or not the perturbation moisture, particularly in PBL, is zonally asymmetric (Sobel and Maloney, 2012, 2013; Jiang et al., 2015; Adames and Kim, 2016; Wang et al., 2017). In the following, we discuss physical mechanisms behind the two moisture mode theories.

Observational analyses showed that while lower-tropospheric moisture anomaly is in phase with MJO convection, PBL moisture anomaly leads the MJO convection (Sperber, 2003; Kiladis et al., 2005; Hsu and Li, 2012). Figure 2 illustrates the composite zonal–vertical distribution of MJO-filtered moisture and its phase relationship with the MJO convection (represented by a negative OLR center). While in the middle troposphere the maximum moisture anomaly is co-located with the MJO convection, in the PBL there is a clear zonal asymmetry in the perturbation moisture field; that is, a positive (negative) center is located to the east (west) of the OLR center. Because of this asymmetry, the maximum moisture content line tilts eastward and downward.

To demonstrate how the PBL moisture asymmetry affects the MJO growth and evolution via atmospheric destabilization, the vertical profile of the intraseasonal equivalent potential temperature (θ_e') was examined by Hsu and Li (2012). As shown in the top panel of Fig. 3, a significant increase of low-level θ_e' is found, consistent with PBL moistening, to the east of the MJO convection. If defining a convective instability parameter as the difference of θ_e' between the PBL (850–1000 hPa) and the middle troposphere (400–500 hPa), one may find that the atmosphere is more (less) potentially unstable to the east (west) of the MJO convective center (bottom panel of Fig. 3). Therefore, a phase leading of a positive low-level moisture anomaly may set up a relatively unstable stratification and generate a favorable environment for potential development of new convection to the east of the MJO convective center.

A moisture budget analysis was conducted to reveal the cause of the PBL moistening in front of MJO convection. The diagnosis result showed that the largest positive contribution is anomalous vertical moisture advection; that is, the advection of the mean moisture (which has a maximum at the surface and decays exponentially with height) by anomalous ascending motion, the latter of which is associated with the PBL convergence. This indicates that the boundary layer convergence and associated ascending motion play an important role in moistening the PBL to the east of deep convection.

Physically, two factors may contribute to the moistening in PBL. The first factor is the boundary layer conver-

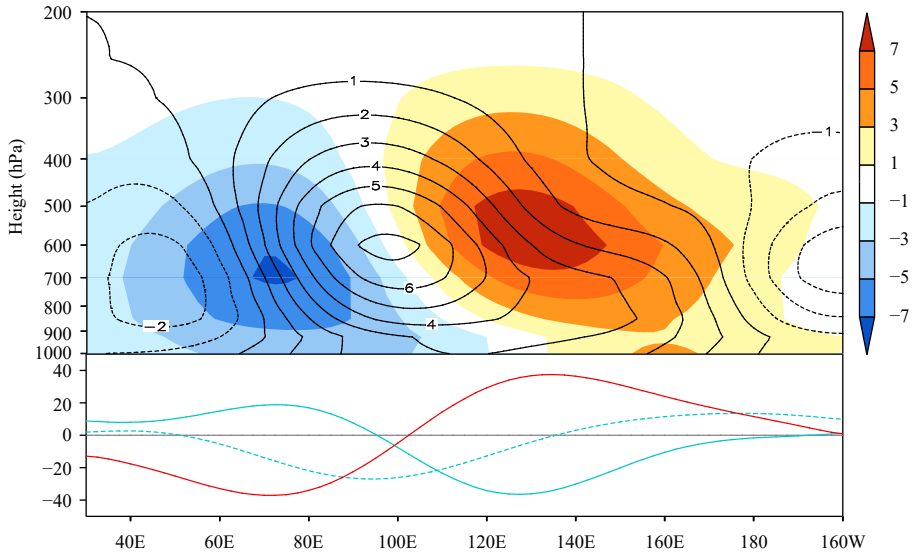

Fig. 2. (Upper panel) Zonal–vertical distributions of 0°–10°S averaged MJO-filtered specific humidity (contour, 10^{-4} kg kg^{-1}) and specific humidity tendency (shading, 10^{-10} kg kg^{-1} s^{-1}). (Bottom panel) Zonal distributions of 0°–10°S averaged MJO-filtered OLR (blue dashed line, W m^{-2}), OLR tendency (blue solid line, 10^{-6} W m^{-2} s^{-1}), and column-integrated specific humidity tendency (red line, 10^{-7} kg m^{-2} s^{-1}) during the active phase of MJO in the eastern Indian Ocean.

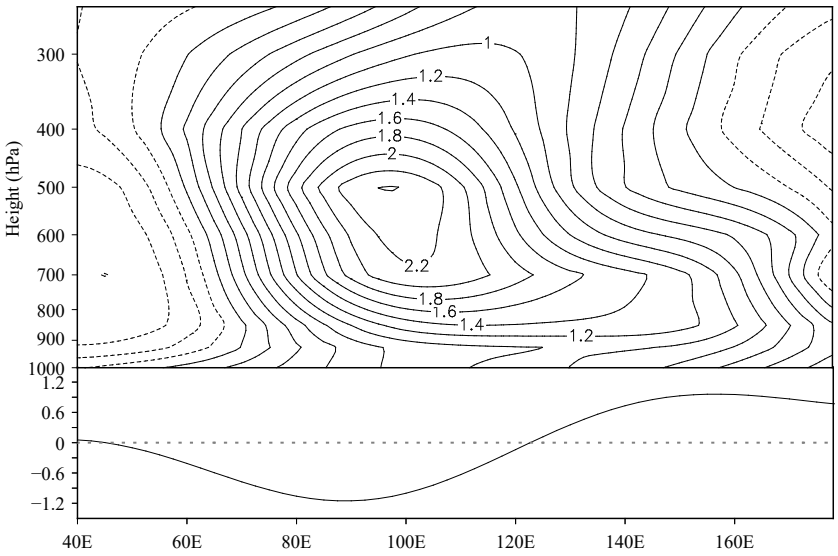

Fig. 3. As in Fig. 2, but for MJO-filtered equivalent potential temperature (θ_e', upper panel) and the convective instability index (bottom panel) defined as the difference of θ_e' between the PBL and the middle troposphere [i.e., 1000–850-hPa averaged θ_e' minus 500–400-hPa averaged θ_e']. Unit: K. From Hsu and Li (2012).

gence, and the second factor is the surface evaporation. Hsu and Li (2012) showed that the low-level convergence presents an eastward shift to the MJO convection, whereas the surface evaporation tends to decrease to the east of MJO convection. The result indicates that the boundary layer convergence is a major process that causes the observed phase leading of PBL moisture.

The decrease of surface evaporation, along with the increase of downward shortwave radiation, leads to the change in SST (Jones and Weare, 1996; Shinoda et al., 1998; Araligidad and Maloney, 2008). As a result, a warm (cold) sea surface temperature anomaly (SSTA) appears to the east (west) of MJO convection.

How does the warm SSTA contribute to the eastward propagation? According to Lindzen and Nigam (1987), a warm SSTA may induce a boundary layer convergence through the change of the boundary layer temperature and pressure. However, it is not clear to what extent the observed PBL convergence is contributed by the underlying SSTA. Figure 4 is a schematic diagram illustrating

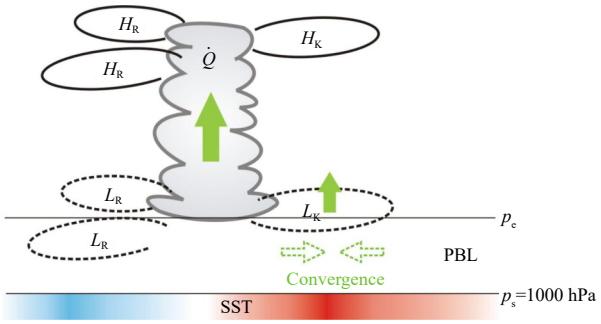

Fig. 4. Schematic diagram of boundary layer convergence induced by free-atmospheric wave dynamic and SSTA. Cloud stands for the MJO convection with heating. Solid (dashed) gyres with H_K (L_K) and H_R (L_R) indicate the high (low) pressure anomaly associated with Kelvin and Rossby waves response to convection, respectively. Red and blue shadings denote the positive and negative SSTAs, respectively. Solid green arrows indicate the anomalous ascending motion, dashed green arrows represent the boundary layer convergence, and p_s and p_e are pressure levels at the bottom and top of the PBL, respectively.

key processes that contribute to the phase leading of the boundary layer convergence. Firstly, the mid-tropospheric heating associated with MJO deep convection induces a baroclinic free-atmosphere response, with a Kelvin (Rossby) wave response to the east (west) of the convective center. The anomalous low pressure at top of the PBL associated with the Kelvin wave response may induce a convergent flow in the boundary layer, while a PBL divergence may occur to the west of the convective center between two Rossby wave gyres. Thus, the first convergence-generation process is associated with the mid-tropospheric heating and equatorial wave responses to the heating. The second generation process is associated with the SSTA forcing. As a warm SSTA is generated to the east of the MJO convection, the warm SSTA may drive boundary layer flows through induced hydrostatic effect on sea level pressure (Lindzen and Nigam, 1987). Therefore, the convergence in the atmospheric boundary layer may be connected to the underlying positive SSTA and associated SSTA gradients to the east of the MJO convection.

To examine quantitatively the relative roles of the SSTA gradient induced pressure gradient force and the heating induced free-atmospheric wave dynamics in determining the PBL convergence, a boundary-layer momentum budget was diagnosed by Hsu and Li (2012). Following Wang and Li (1993), the PBL momentum equation may be written as

$$f\boldsymbol{k}\times\boldsymbol{V}_{\mathrm{B}}'+E\boldsymbol{V}_{\mathrm{B}}'=-\nabla\phi_{\mathrm{e}}'+\frac{R}{2}\frac{(p_{\mathrm{s}}-p_{\mathrm{e}})}{p_{\mathrm{e}}}\nabla T_{\mathrm{s}}', \qquad (1)$$

where a prime denotes the MJO component, f is the Coriolis parameter, $\boldsymbol{k}$ is the unit vector in the vertical direction, $\boldsymbol{V}_{\mathrm{B}}$ denotes the vertically averaged horizontal wind in the boundary layer, ∇ is the horizontal gradient operator, ϕ_e denotes the geopotential at the top of the boundary layer, R is the gas constant of air, p_{s} and p_{e} are pressures at the bottom and top of the PBL respectively, T_{s} is the surface temperature, and E is the friction coefficient (equal to 10^{-5} s^{-1}). The first term in the right hand side of Eq. (1) represents the free-atmospheric wave effect. The second term in the right hand side of Eq. (1) represents the SSTA forcing effect. To test the sensitivity of the result to the boundary layer depth, two different PBL depths, 1000–850 and 1000–700 hPa, are applied.

Figure 5 reveals the diagnosis results for the PBL convergence. The free atmospheric wave effect in response to the MJO heating plays a major role in determining the boundary layer convergence. It accounts for 90% and 75% of the total boundary layer convergence in the case of p_{e} = 850 and p_{e} = 700, respectively. The warm SSTA induced by decreased latent heat flux ahead of MJO convection, on the other hand, also plays a role. It contributes about 10%–25% to the observed boundary layer convergence. Since the PBL convergence is a major factor affecting the moisture asymmetry, the result above suggests that both the heating induced equatorial wave response and the underlying SSTA contribute to the eastward propagation of MJO.

The second type of the moisture mode theory excludes the aforementioned asymmetric PBL moisture effect but emphasizes the zonal asymmetry of column integrated MSE tendency. To unveil dynamics behind MJO eastward propagation, Wang et al. (2017) conducted an MSE budget for observations and outputs from 27 global models that are separated into good and poor MJO groups based on their 20-yr simulation performance.

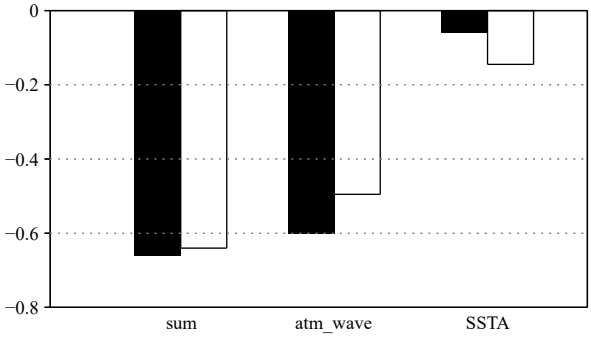

Fig. 5. (From left to right) Total boundary layer convergence (sum) averaged over 0°–10°S, 130°–150°E, induced by both the free-atmospheric wave dynamic (atm_wave) and SSTA, and relative contributions of wave dynamic and SSTA effect in the case of p_{e} = 850 (filled bars) and p_{e} = 700 hPa (hollow bars). Unit: 10^{-6} s^{-1}. From Hsu and Li (2012).

MSE (m) is defined as $m = c_pT + gz + L_vq$, where T is temperature, z is height, q is specific humidity, c_p is the specific heat at constant pressure (1004 J K^{-1} kg^{-1}), g is the gravitational acceleration (9.8 m s^{-2}), and L_v is the latent heat of vaporization (2.5 × 10^6 J kg^{-1}). The column-integrated MSE budget can be written following Neelin and Held (1987) as

$$\langle \partial_t m \rangle = -\left\langle \omega \partial_p m \right\rangle - \langle \boldsymbol{V} \cdot \nabla m \rangle + Q_t + Q_r, \qquad (2)$$

where the angle bracket represents a mass-weighted vertical integral from the surface to 100 hPa, p is pressure, $\boldsymbol{V}$ is horizontal wind vector, and ω is pressure velocity. The left-hand-side term represents MSE tendency, the first and second terms on the right-hand-side represent the vertical and horizontal advection, respectively. Q_t represents the sum of surface latent and sensible heat fluxes, and Q_r represents the sum of vertically integrated shortwave and longwave heating rates. For the observational diagnosis, Q_r is calculated from MERRA (Modern Era Retrospective Analysis for Research and Applications) and the other terms are derived from ERA_I (ECMWF Interim Reanalysis) data.

Figure 6 (upper panels) shows lagged time–longitude diagrams of regressed rainfall and column MSE anomalies for the observation as well as good and poor model groups. A marked feature from the observation is that column integrated MSE anomaly is approximately in phase with the rainfall anomaly and they both show clear eastward propagation (Fig. 6a). For the good models (Fig. 6b), a robust eastward-propagating intraseasonal mode is visible, which has a feature similar to the observation. By contrast, eastward propagation is not seen in the poor model composite (Fig. 6c). The result implies that to the first order of approximation, MJO convective anomaly may be regarded as an MSE envelope, moving eastward.

To examine what causes the eastward movement of the column integrated MSE anomaly, one may examine the horizontal pattern of the MSE tendency at a given time. The horizontal patterns of the MSE tendency anomaly (shaded) overlaid by the MSE anomaly (contour) at day 0 are shown in lower panels of Fig. 6. Both the ob-

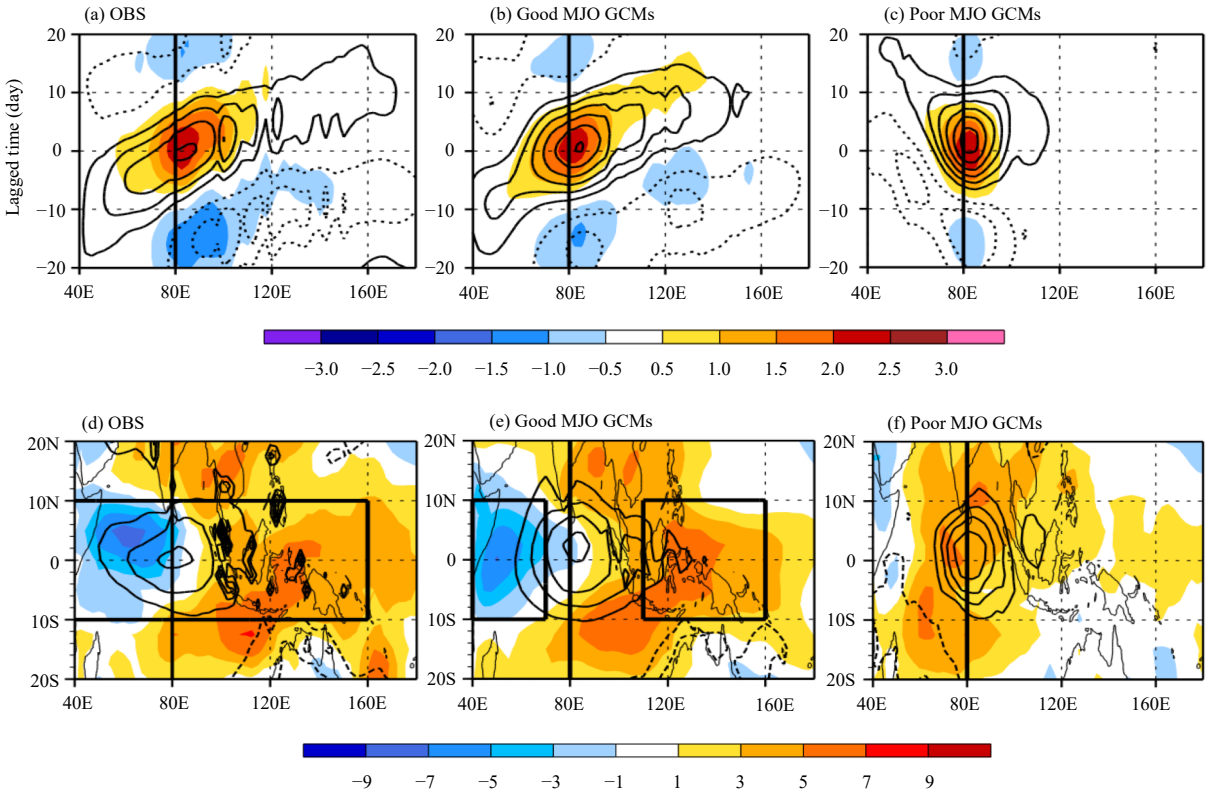

Fig. 6. (Upper panels) Longitude–time evolution of rainfall anomalies (shaded, mm day^{-1}) and column-integrated Moist Static Energy (MSE) anomalies (contour, J m^{-2}; contour interval is 1 × 10^6, with zero line omitted) averaged over 10°S–10°N by lag regression against 20–100-day band-pass-filtered anomalous rainfall averaged over the equatorial eastern Indian Ocean (5°S–5°N, 75°–85°E). (Lower panels) Regressed day 0 column-integrated MSE tendency anomaly (shaded, W m^{-2}) overlaid by MSE anomaly itself (contour, J m^{-2}; contour interval is 2 × 10^6, with zero line omitted). (a, d) are calculated from GPCP observation and ERA_I reanalysis, (b, e) are the good MJO model composite, and (c, f) are the poor MJO model composite. The rectangle in (d) marks the projection domain (10°S–10°N, 40°–160°E). From Wang et al. (2017).

servation and the good model composite show a positive tendency anomaly to the east of maximum MSE anomaly center and a negative tendency anomaly to the west. Such zonal asymmetry of the MSE tendency favors the eastward propagation of the MSE maximum. The poor model composite, however, does not have a clear zonal asymmetry in the MSE tendency distribution. In these poor models, a positive tendency anomaly is observed flanking both sides of the MSE maximum, and the tendency to the west is even slightly stronger than that to the east, possibly explaining the hint of slight westward propagation shown in Fig. 6c.

Since the MJO tendency is controlled by four terms in the right hand side of Eq. (2), a natural question is what causes the observed asymmetry of the MSE tendency. Wang et al. (2017) projected each of the terms onto the observed MSE tendency field over the domain of 10°S–10°N, 40°–160°E shown in Fig. 6d. If a tendency term has a similar asymmetric pattern as in Fig. 6d, the projection coefficient should be a positive value. If a tendency term is exactly the same as that shown in Fig. 6d, the projection coefficient should be equal to 1. Thus, the projection coefficient can be used to measure whether or not and to what extent a term may contribute to the eastward propagation. Through this projection analysis, one may diagnose the fractional contribution of each budget term to the observed asymmetric MSE tendency.

Figure 7 shows the projection coefficients from the ERA-I reanalysis and from the good and poor model group composites as well as their difference. Based on the observational diagnosis, one may see clearly that both horizontal and vertical MSE advection terms contribute to MJO eastward propagation, while the surface heat flux and column integrated atmospheric radiation terms contribute to westward propagation. A net effect of these terms causes a slow eastward phase speed (Li and Hu, 2019).

In the good model composite, the vertical and horizontal advections show positive coefficients with comparable magnitudes with the observation. Q_t and Q_r show negative coefficients, indicating that they hinder the eastward propagation. These results are in good agreement with the observations (Fig. 7a). By contrast, the poor model group presents negative projections for the vertical advection (blue bar, Fig. 7c) and much weaker projection for the horizontal advection (pink bar, Fig. 7c), compared to the good model group. The near-zero projection of MSE tendency (black bar, Fig. 7c) in the poor model composite is thus primarily a consequence of both the reversed sign of vertical advection and the weaker

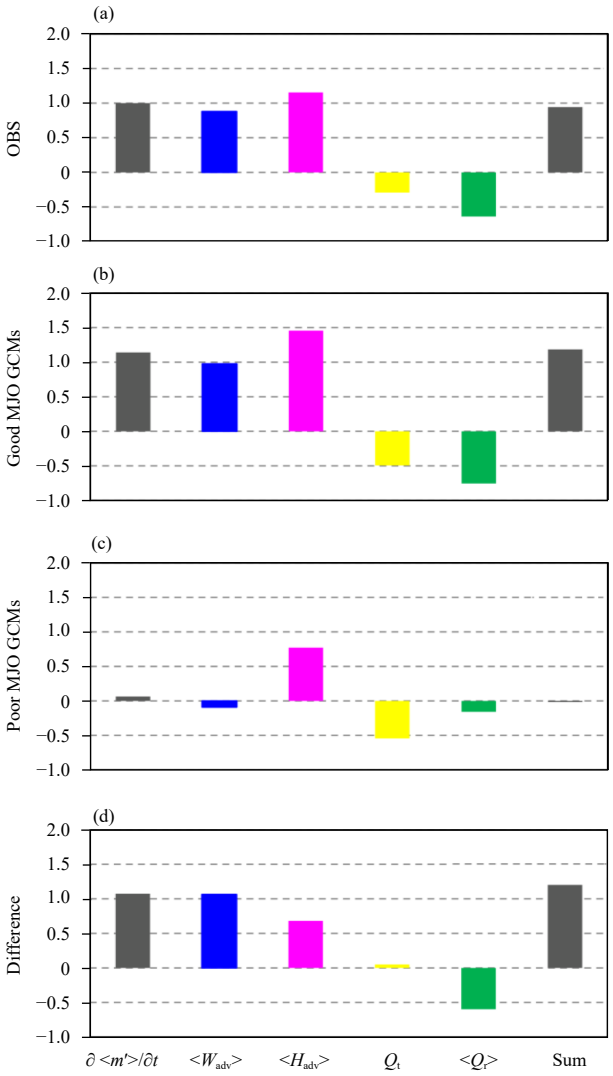

Fig. 7. Projection of regressed column-integrated MSE budget terms against the observed MSE tendency anomaly at day 0 over 10°S–10°N, 40°–160°E. Bars from left to right represent MSE tendency, vertical advection (W_{adv}), horizontal advection (H_{adv}), turbulent heat fluxes (Q_t), radiation heating rate (Q_r) and sum of budget terms (Sum). (a) is calculated from ERA-I reanalysis, and (b) and (c) are the good and the poor model composite, respectively. (d) is the difference between the good and poor composite results (good minus poor). From Wang et al. (2017).

horizontal advection projection. Figure 7d shows the difference of MSE budget terms between the good and the poor model composites. As one can see, the difference is primarily attributed to the vertical MSE advection, followed by the horizontal MSE advection.

How do the vertical and horizontal advection terms contribute to MJO eastward propagation? Figure 8 is a schematic diagram illustrating how this mechanism works (see Wang et al., 2017 for detailed description). To the east of the MJO convection, downward anomaly appears in the upper troposphere and upward anomaly

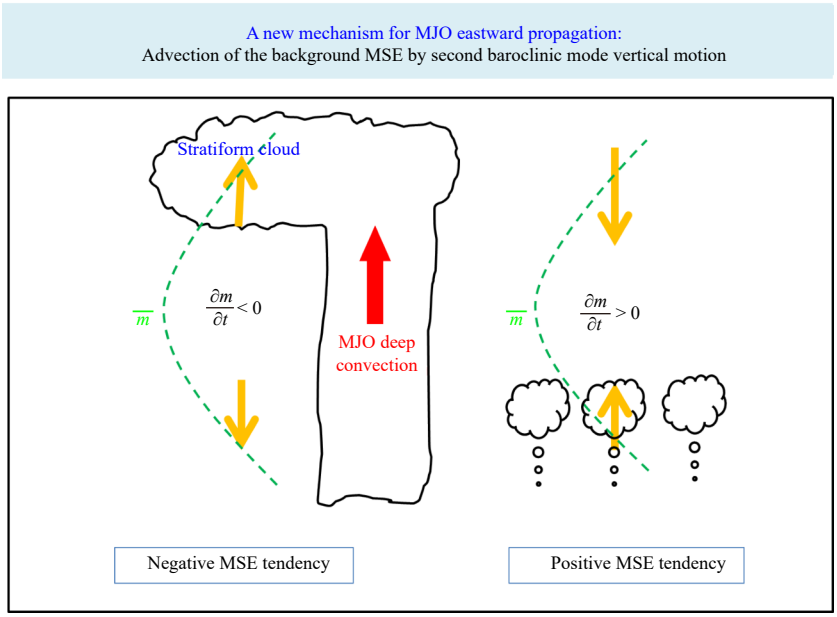

Fig. 8. Schematic diagram illustrating the role of anomalous vertical MSE advection in generating a zonal asymmetric MSE tendency. The tall cloud describes gross feature of an MJO, which has a large-scale deep convection over its center and a stratiform cloud-like structure in the rear in the upper troposphere. The small clouds to the east of MJO convection indicate the shallow convection. The green curves denote climatological mean MSE profiles. The orange arrows denote the second baroclinic mode vertical velocity anomalies.

appears in the lower troposphere; to the west, upward anomaly in association with stratiform cloud appears in the upper troposphere while downward anomaly appears in the lower troposphere. Given that the mean MSE profile minimizes in the middle troposphere, such a distribution of second-baroclinic mode vertical velocity anomalies would induce a positive (negative) column-integrated MSE advection to the east (west), promoting the eastward propagation of MJO. Wang et al. (2017) demonstrated that the existence of stratiform cloud in the rear of the MJO convection is critical in generating zonally asymmetric vertical motion distribution in the upper troposphere.

While the vertical MSE advection is primarily attributed to upper tropospheric process, the horizontal advection is mainly determined by meridional MSE advection in the lower troposphere (Wang et al., 2017). Figure 9 shows a schematic diagram of this mechanism. In response to MJO heating, lower tropospheric easterly anomalies associated with Kelvin wave response are generated. Decent anomalies appear to the east in association with this Kelvin wave response, which induces a negative heating anomaly in situ. The negative heating further induces an anticyclonic Rossby gyre with poleward flows in the lower troposphere. The poleward flows cause a positive MSE advection because maximum mean MSE appears near the equator. Thus, a positive MSE tendency appears to the east of MJO convection. Meanwhile, low-level cyclonic flows to the west associated with Rossby

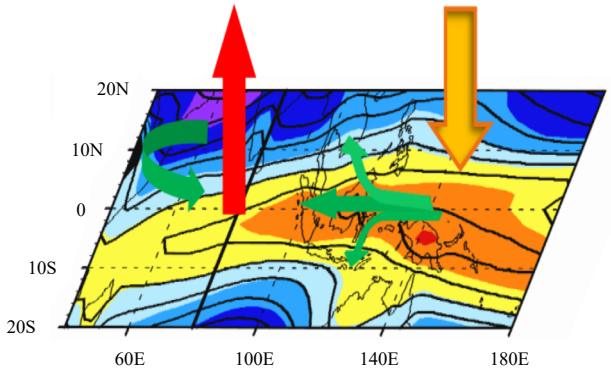

Fig. 9. Schematic representation of key processes through which the zonal asymmetry of anomalous horizontal MSE advection is generated. The shaded and contour denote the horizontal distribution of boreal winter mean humidity and MSE averaged over 600–800 hPa. The green arrows denote the key anomalous flows in the lower troposphere that induce positive (negative) MSE advection to the east (west). The red arrow at 80°E denotes ascending motion or positive heating associated with MJO deep convection while the orange arrow over the western Pacific Ocean denotes descending motion or negative heating in association with Kelvin wave response.

wave response advect low MSE air equatorward, leading to a negative MSE tendency. The processes above lead to the east–west asymmetry of the column integrated MSE tendency, promoting eastward propagation (Kim et al., 2014).

3.2 *Mechanisms for MJO initiation*

Observational analyses (e.g., Zhao et al., 2013) showed

that MJO convection is often initiated over the western equatorial Indian Ocean (WIO). A long-term hypothesis is that MJO initiation arises from the circumnavigation of a preceding MJO event that travels around the global tropics (e.g., Lau and Peng, 1987; Wang and Li, 1994; Matthews, 2000, 2008; Seo and Kim, 2003). The promise behind the circumnavigating hypothesis is that the eastward-propagating upper-tropospheric divergence signal associated with MJO may trigger deep convection over relatively moist and warm Indian Ocean after it passes the African continent. As demonstrated by idealized numerical model experiments (Zhao et al., 2013) and observational analyses (Li et al., 2015), this circumnavigating process is not crucial for MJO initiation.

Based on a 20-yr observational data analysis, two major initiation mechanisms were proposed by Zhao et al. (2013). The first one is relevant to successive MJO events, that is, a suppressed-phase MJO, after it moves to eastern IO, may trigger a convective-phase MJO, through the low-level horizontal moisture advection. Figure 10 presents the horizontal patterns of the mean specific humidity field and the MJO wind perturbation field derived based on a 10-day average prior to MJO convective initiation in WIO. As expected, maximum mean specific humidity is located over EIO, where SST is higher compared to WIO. The MJO flow during the initiation period is dominated by anomalous easterlies and two anticyclonic Rossby gyres over the tropical IO. Such a wind anomaly resembles the Gill (1980) pattern and is typically observed when the suppressed MJO convection is located in the EIO. The easterly anomalies advect the high mean moisture westward, leading to the increase of the lower-tropospheric moisture over the initiation region (20°S–0°, 50°–70°E).

The second initiation mechanism is through extratropical or midlatitude wave processes, a mechanism possibly applicable to primary MJO events. A case study by Hsu et al. (1990) suggested a possible midlatitude wave source from the Northern Hemisphere (NH). Such a hypothesis, however, was challenged by Zhao et al. (2013), who pointed out, based on their idealized numerical model experiments, that the Southern Hemispheric Rossby wave forcing is more critical. Although the NH wave activity is stronger in boreal winter, it is difficult for wave fluxes to cross the equator, and thus hardly for them to affect MJO initiation, which happens south of the equator.

To obtain the statistically robust signal of the midlatitude impact, Zhao et al. (2013) examined the upper tropospheric (200-hPa) geopotential height anomaly pattern

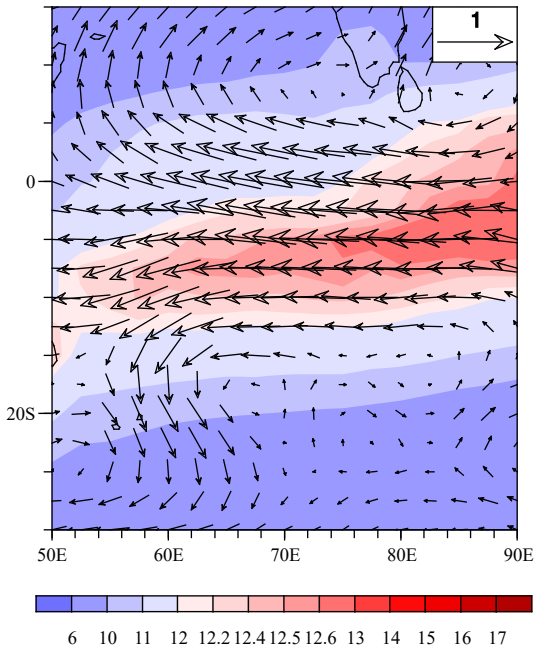

Fig. 10. Vertically (1000–700-hPa) integrated intraseasonal wind (vector, m s^{-1}) and the low-frequency background state specific humidity (shaded, g kg^{-1}), averaged during the initiation period (from day –10 to day 0, with day 0 defined as the time when the area-averaged OLR anomaly over the WIO initiation region switches its sign from a positive to a negative value). From Zhao et al. (2013).

and associated wave activity flux during the MJO initiation period using the same 20-yr reanalysis data (Fig. 11). Note that the geopotential height anomaly displays a wave train pattern, with high pressure centers located southeast of South America and southeast of Africa, and low pressure centers in between and to the east of Madagascar. There are pronounced eastward wave activity fluxes over midlatitude Southern Hemisphere (SH), indicating that the Rossby wave energy propagates eastward. The eastward wave activity fluxes turn northward and converge onto the tropical IO. The wave flux convergence implies that the wave energy is accumulated over the region. Thus, SH midlatitude Rossby wave perturbations may trigger MJO initiation in the tropical IO through wave energy accumulation process.

The third initiation mechanism is through air–sea interaction process. Li et al. (2008) proposed a delayed air–sea interaction mechanism in which a preceding active phase MJO may trigger an inactive phase MJO through a delayed effect of induced SSTA over the IO. Figure 12 shows the evolution of the 20–90-day filtered SST, wind stress, and OLR anomalies during a composite MJO cycle over the IO in northern winter (DJF). The regression is based on 20–90-day band-pass filtered zonal wind stress averaged over the domain of 5°–12.5°S,

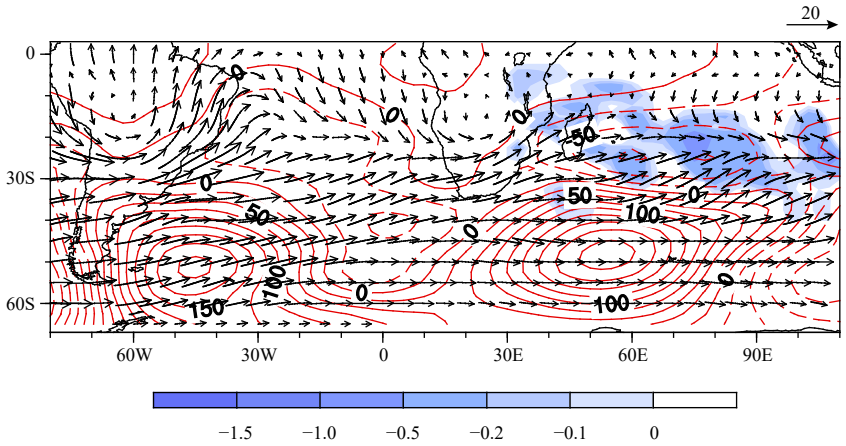

Fig. 11. The observed 20–90-day filtered geopotential height anomaly (contour, $m^2\ s^{-2}$), Rossby wave activity flux (vector, $m^2\ s^{-2}$), and wave flux divergence (shaded, $10^{-5}\ m\ s^{-2}$; only negative values are shaded over the Indian Ocean) at 200 hPa during the initiation period from day –10 to day 0. From Zhao et al. (2013).

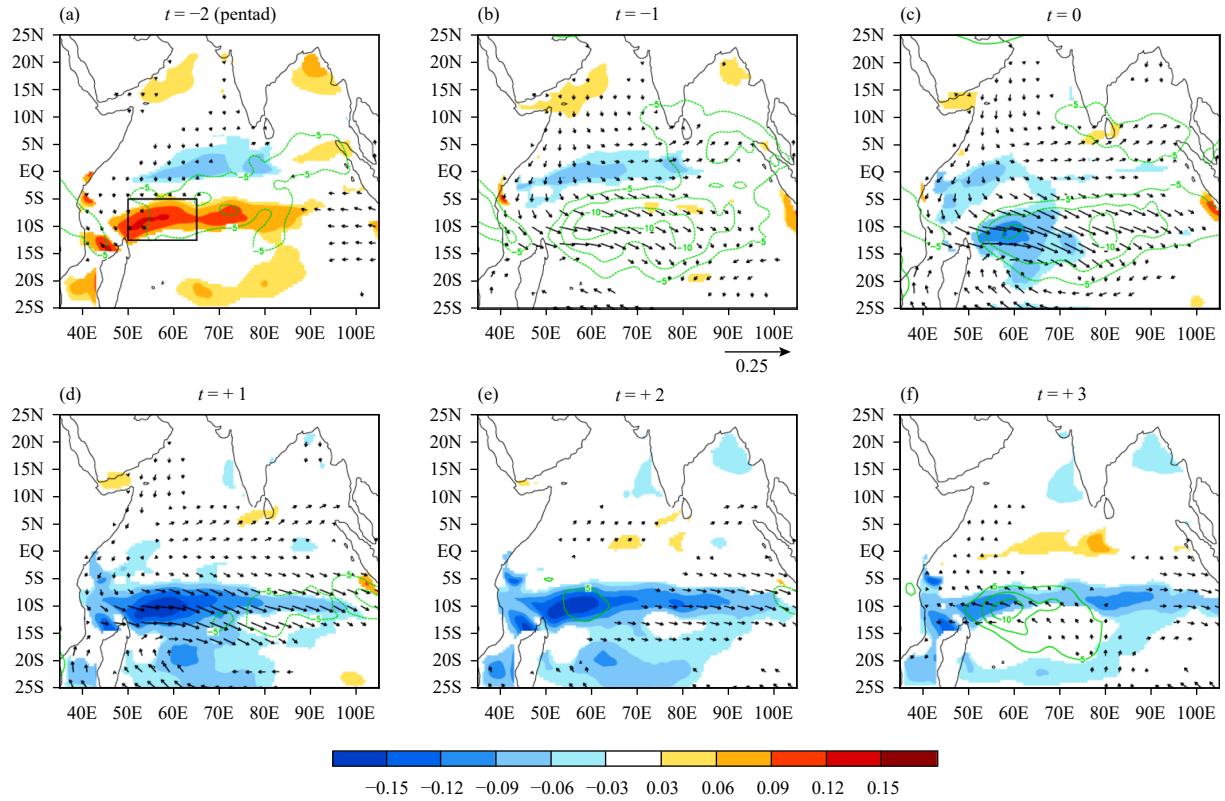

Fig. 12. Regressed SST (shading, K), wind stress (arrow), and OLR (solid contours for positive and dashed contours for negative values; starting from ± 5 W m^{-2}, interval: 2.5 W m^{-2}) anomalies for the lag of pentad (a) –2, (b) –1, (c) 0, (d) +1, (e) +2, and (f) +3 for northern winter (DJF) season. Only wind stress and SST (OLR) anomalies that exceed 95% (90%) significance level are shown.

50°–65°E. All fields shown in Fig. 12 are regressed onto the index. A warm SSTA appears along 10°S in pentad –2, due to a delayed ocean response to a preceding suppressed phase MJO. In pentad –1, westerly wind stress and negative OLR signals associated with an active phase of MJO appear in the tropical IO. This leads to rapid decrease of the initial warm SSTA due to both the increased surface latent heat flux and reduced shortwave radiation associated with the active phase MJO. Because background mean wind is westerly along 10°S, a positive westerly anomaly increases evaporative cooling in the region. This gives rise to the in-phase relationship between the anomalous surface shortwave radiation and the latent heat flux, and together they act with the ocean

entrainment to strongly cool the SST. As a result, a cold SSTA appears along 10°S in pentad 0. In pentad +1, the cold SSTA is enhanced over the western to central IO along approximately 10°S (see Fig. 12). One pentad later, a positive OLR anomaly appears at about 55°E, collocated with the cold SSTA there. The positive OLR anomaly subsequently expands eastward and grows. It is noteworthy that suppressed convection tends to develop over the location where cold SSTA is already present for 5 to 10 days, as inferred from the sequence of charts from pentad +1 to +3. This phase relationship between the SST and convection implies a delayed air–sea interaction scenario for MJO initiation; that is, on the one hand, an ocean cooling is induced by the wet phase of the MJO through combined cloud radiative forcing and surface evaporation/ocean vertical mixing, and on the other hand, the so-induced WIO cold SSTA in turn initiates a subsequent dry phase of the MJO. Thus, air–sea interactions play an important role in the re-initiation of the MJO over the WIO in boreal winter.

This ocean feedback mechanism was recently confirmed with a long-term integration of a coupled general circulation model (Chang et al., 2019). The ocean feedback process becomes less effective in boreal summer when the mean SST is low in western IO and intraseasonal SST variability in the IO is weaker (Zhang et al., 2019).

4. Impact of MJO on East Asian climate

A great example of MJO impact on East Asian extreme weather is the continuous occurrence of four ice storms in South China during a 23-day period (from 10 January to 2 February 2008). The storms led to the broken of electronic cable lines and collapse of high speed train transportation systems, causing millions of people stranded in train stations. The total economic loss is more than 100 billion Chinese Yuan.

Hong and Li (2009) found that the persistent ice storms resulted from the combined effect of tropical and high-latitude low-frequency forcing. The Hovmöller diagram of the OLR anomaly averaged over 15°S–5°N shows two eastward-propagation convective-phase MJO signals (see arrows in Fig. 13a) and a dry phase MJO signal that happened in between. The dry phase MJO stayed over Maritime Continent from early January to 1 February. The spatial patterns of OLR and associated low-level wind anomalies averaged during the dry phase are shown in Fig. 13b. Note that in the dry phase the convection over Sumatra was suppressed. Near the equator, easterly anomalies occurred from the coast of Sumatra to Madagascar while southerly anomalies appeared over the Bay of Bengal and the South China Sea. These southerly anomalies were critical in transporting abundant moisture from the tropical oceans to South China.

Meanwhile, there was a persistent high pressure anomaly over the Siberian region in high latitudes. Figure 13c illustrates the time series of the Siberian high index defined as the averaged sea-level pressure (SLP) over 40°–60°N, 80°–120°E. As one can see, the high surface pressure anomaly persisted from middle of January all the way to middle of February. Associated with this strong, persistent positive SLP anomaly were continuous northerly anomalies that transported cold polar air mass southward.

The combined forcing of moist and warm southerlies associated with tropical MJO and cold and dry northerlies from high latitudes associated with the Siberian high led to occurrence of the devastating, persistent ice storms during the 23-day period. The analysis result implies that an accurate long-lead forecast of such an extreme weather event requires a model that is able to capture both the tropical and high-latitude intraseasonal oscillations.

During its eastward propagation, MJO convection could generate an extratropical Rossby wave train that emanates from the tropics toward high latitudes, which could then induce remote responses in precipitation over China. The spatial pattern of these responses is very different in different seasons and different phases of the MJO due to changes in the atmospheric background state and the location of the MJO convection center. Generally speaking, MJO exerts great impacts on the precipitation and circulation in China, especially over its eastern part (Zhang et al., 2009; Bai et al., 2011; Jia et al., 2011).

Anomalous precipitation exhibits systematic changes in the Yangtze River basin and South China during the eastward propagation of the MJO in boreal winter (Jia et al., 2011). Figure 14a shows the composites of regional mean precipitation anomalies and its departure percentage over Southeast China (east of 105°E and south of 32.5°N over China) for 8 MJO phases based on the Real-time Multivariate MJO (RMM) index. When the MJO convection center is located over the Indian Ocean (phases 2 and 3), precipitation over the eastern China is significantly enhanced, while it is dramatically suppressed when the MJO convection center appears over the western Pacific (phases 6 and 7).

The impacts of MJO on winter precipitation over China are mainly through its influence on the northward moisture transport originated from the Bay of Bengal and the South China Sea by modulating the southern trough

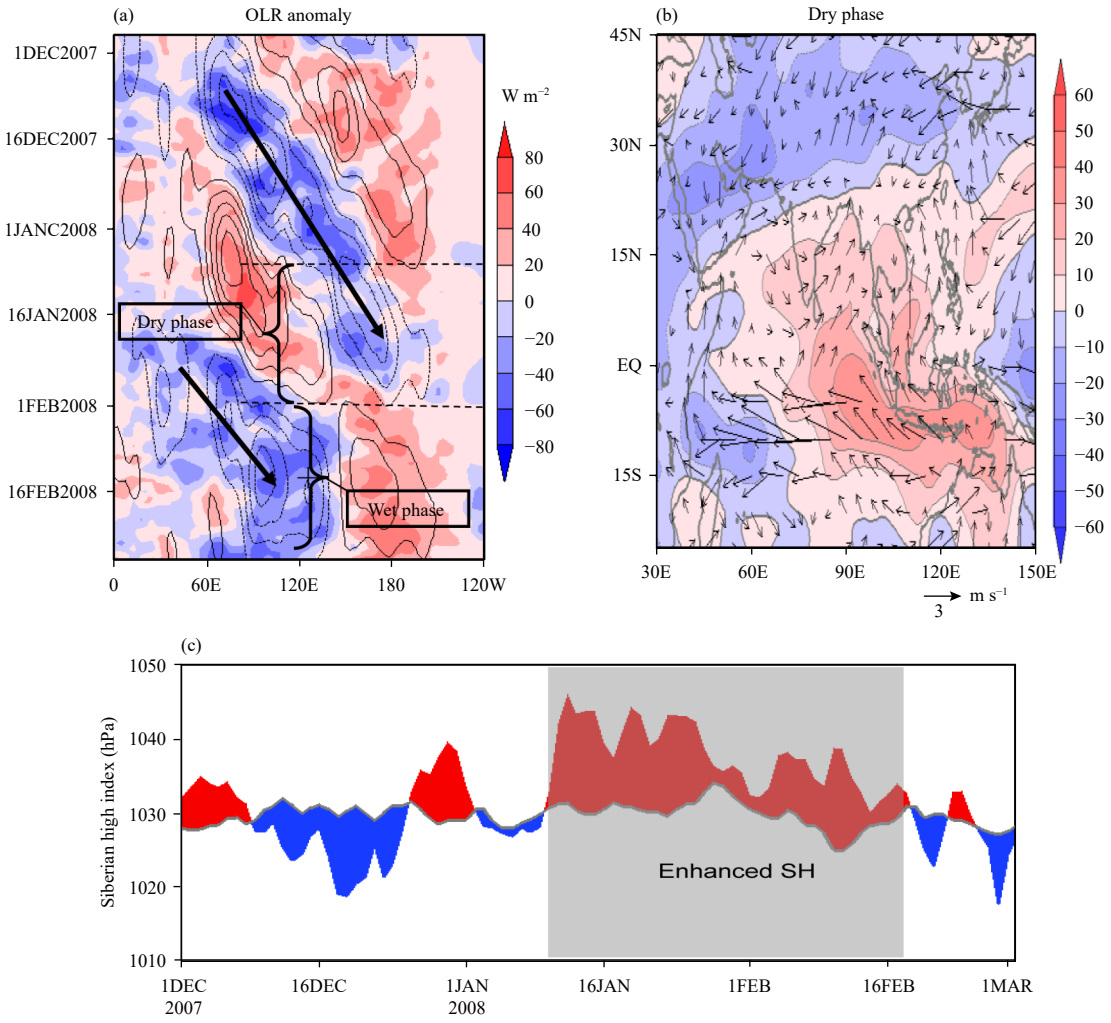

Fig. 13. (a) Hovmüller diagram of 20–70-day filtered OLR anomaly (contour, interval: 20 W m^{-2}) averaged over 15°S–5°N. Shading denotes the raw data. (b) Horizontal distribution of the 20–70-day filtered OLR anomaly (shaded) and 925-hPa wind anomaly (vector) fields averaged during the MJO dry phase shown in (a). (c) Time series of the Siberian high index defined as the averaged SLP over 40°–60°N, 80°–120°E. Red (blue) shaded region represents the index higher (lower) than the long-term climatology. From Hong and Li (2009).

over the Bay of Bengal (Fig. 14b) and the western Pacific subtropical high in the subtropics (figure omitted). Furthermore, MJO can also modulate the East Asian winter monsoon in the midlatitude (Fig. 14c), which further impacts the precipitation over East China.

The positive precipitation anomalies over the Yangtze River basin in eastern China is also enhanced when the MJO convection center is over the Indian Ocean, and the positive precipitation anomalies could cover the whole part of Southeast China but with weaker amplitude later when MJO moves to the Maritime Continent in boreal spring (Bai et al., 2011). Almost same distinct transition of precipitation anomaly from being enhanced to being suppressed as that in boreal winter is found in Southeast China during boreal summer as the MJO convective center moves from the Indian Ocean to the western Pacific (Zhang et al., 2009). During boreal summer when the northward propagation of intraseasonal oscillation prevails, the impact of MJO on the precipitation becomes complicated. The anomalous precipitation over Southeast China reaches its maximum in phase 4 during boreal summer while it is in phase 2 in boreal winter. During boreal summer, MJO impacts the precipitation in Southeast China mainly through the western Pacific subtropical high (WPSH), which could modulate the moisture transport to China. When the MJO convection center is over the Indian Ocean, the WPSH shifts farther westward, and the moisture and upward motion in Southeast China are enhanced. In contrast, when the MJO convection enters the western Pacific, the WPSH retreats eastward, and the moisture and upward motion in Southeast China are weakened (Zhang et al., 2009).

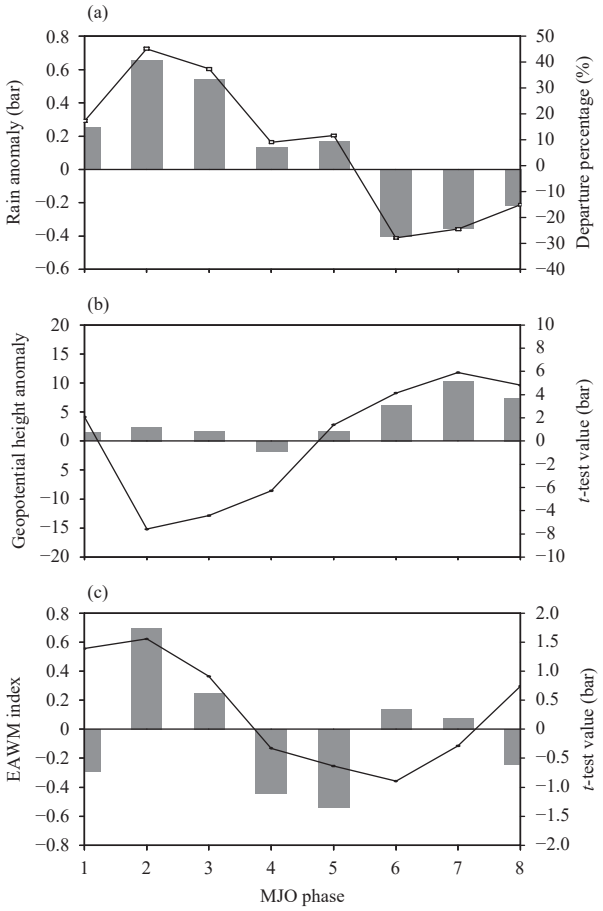

Fig. 14. Composites of anomalous regional mean (a) rainfall (bars, mm day^{-1}) and its departure percentage (line, %) over Southeast China, (b) geopotential height of the southern trough over the Bay of Bengal (15°–25°N, 85°–95°E, line), and (c) the East Asian winter monsoon (EAWM) index (line) for 8 MJO phases. The bar in (b) and (c) indicates the value that *t*-test value minus which at the 95% confidence level; therefore, positive value indicates that the composite for corresponding MJO phase exceeds the 95% confidence level. (From Figs. 6, 8, and 13 in Jia et al. 2011).

The MJO activity influences not only the winter precipitation (Jia et al., 2011; Yao et al., 2015) but also the persistent heavy rainfall (PHR) events during boreal winter in South China (Liu and Hsu, 2019). The PHR event in Liu and Hsu (2019) was defined when rainfall was above the 90th percentile of climatological wintertime rainfall and persisted for three or more days. Similar to the findings of Jia et al. (2011), the MJO show significant influences on the occurrence and total rainfall amount of PHR events via modulating the large-scale background conditions. During phases 1–4, when the MJO convections occur over the equatorial Indian Ocean, the low-level moisture convergence anomaly is observed in southeastern China (SC; 21°–26°N, 108°–120°E) while anomalous divergence of moisture flux appears to the north (Fig. 15c). These conditions favor an increase in PHR amounts over the SC but limit the PHR in the Yangtze River valley (YR; 28°–30°N, 113°–122°E) (Figs. 15a, b). In contrast, decreased (increased) PHP amounts are detected over the SC (YR) when the divergence (convergence) of moisture flux anomalies in the SC (YR) is associated with the western equatorial Pacific MJO convections (phases 5–8) (Figs. 15d–f). The wintertime PHR has experienced a long-term change over the past three decades (1979–2011) with a decreasing (an increasing) trend of PHR amount in the SC (YR). The change in PHR amount at the decadal timescale shows insignificant relationship with sea surface temperature anomalies over the globe. Instead, it seems to be closely linked with the decadal changes in MJO activity. Compared to the earlier epoch (1979–1994), the Indian Ocean (western Pacific) MJO convections along with anomalous moisture convergence (divergence) in the SC occurred less (more) frequently in the recent epoch of 1995–2011 (Fig. 16b). This condition could lead to unfavorable conditions for SC PHR during winter season of 1995–2011 (Fig. 16a). At the same time, the enhancement of moisture convergence associated with the increased frequency of active western Pacific MJO convections in the recent epoch (1995–2011) may contribute to the increased YR PHR (Fig. 16).

The ISO moves away from the equator into the Asian monsoon region during boreal summer; its propagation and phase evolution affect the variations of regional monsoon rainfall by altering background conditions for related weather systems (Yasunari, 1980; Hartmann and Michelsen, 1989; Annamalai and Slingo, 2001; Zhang et al., 2009). In the East Asian monsoon region, several flooding events that occurred in the Yangtze River basin and southern China were found to be associated with the northward-propagating BSISO, including the quasi-biweekly oscillation (QBWO) (Yang and Li, 2003; Zhu et al., 2003; Mao et al., 2010; Liu et al., 2014). Hsu et al. (2016) analyzed quantitatively the influences of lower-frequency BSISO (i.e., 30–60-day ISO, referred to as BSISO1) and higher-frequency BSISO (i.e., 10–30-day QBWO, referred to as BSISO2) on the occurrence probability of precipitation extreme events in southern China. They found that the probability of extreme rainfall occurrences increases (decreases) by 30%–60% relative to climatological state when the moisture convergence (divergence) anomalies induced by BSISO1/BSISO2 were observed in southern China. The BSISO1 is more favorable for the occurrence of extreme precipitation events over inland China (such as the Yangtze–Huai River basin), while the BSISO2 tends to exert a larger influence on rainfall extremes along the southeast coast of

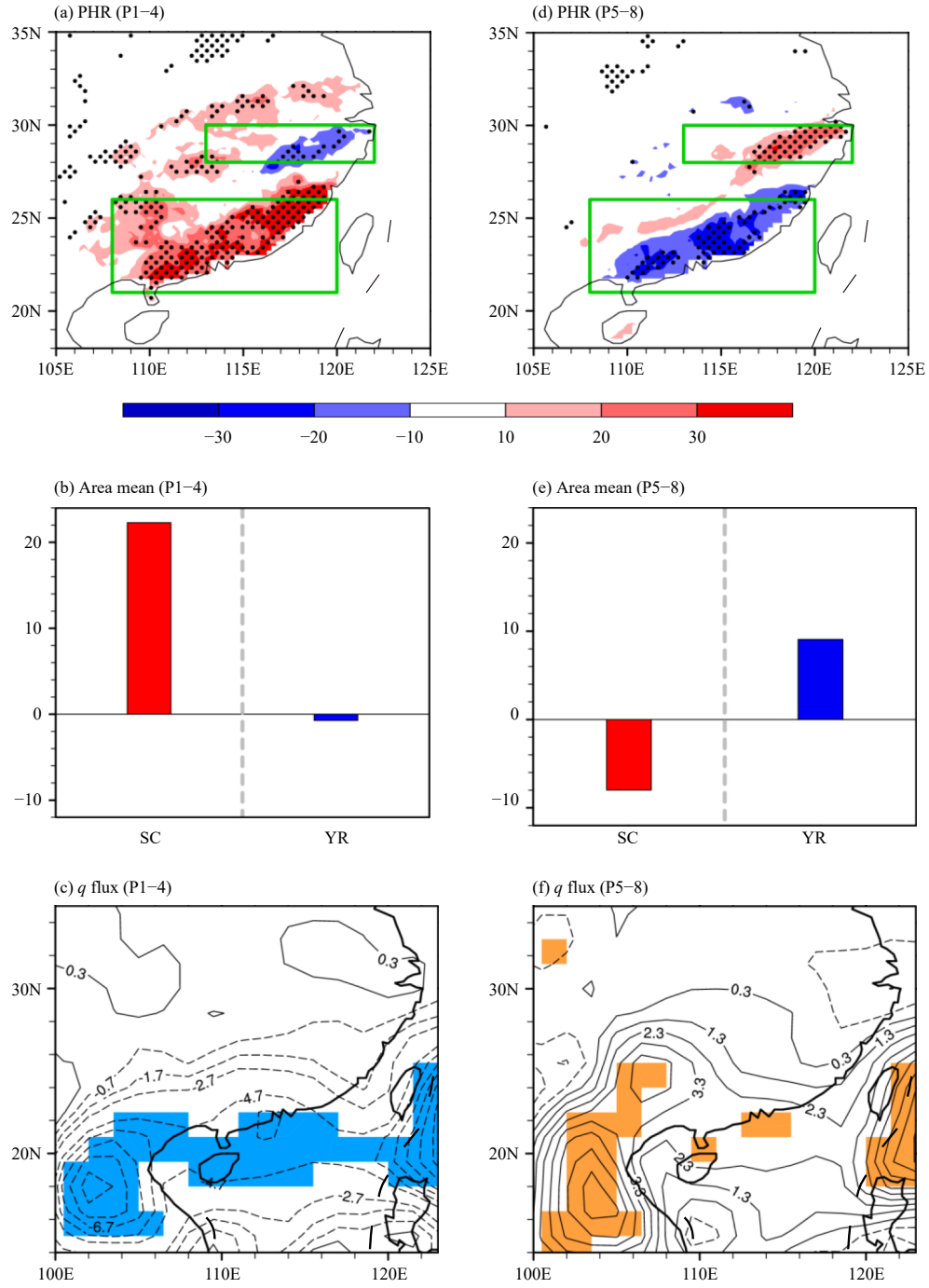

Fig. 15. (a) Anomalies of DJF persistent heavy rainfall (PHR) amount [mm (90 day)$^{-1}$] during phases 1–4 (P1–4) of MJO relative to climatological state. Stippling indicates that the change of PHR amount is statistically significant at the 90% confidence level. (b) Area-averaged wintertime (DJF) PHR amount anomalies [mm (90 day)$^{-1}$] during MJO phases 1–4 (P1–4) over southeastern China (red bar; SC: 21°–26°N, 108°–120°E) and Yangtze River valley (blue bar; YR: 28°–30°N, 113°–122°E). (c) is the same as (a), but for the 1000–850-hPa integrated moisture (q) flux in each winter (contour, 10^{-8} kg cm^{-2} s^{-1}). Shading marks the areas with changes significant at the 90% confidence level. (d)–(f) are the same as (a)–(c), except for the composites of phases 5–8 (P5–8) of MJO.

South China (Fig. 17). The results suggest a potential for monitoring and extended-range forecasting of extreme precipitation events in southern China based on the states of BSISO.

Besides rainfall extreme, recent studies revealed the modulation of East Asian heatwave events by the BSISO (Chen and Zhai, 2017; Hsu et al., 2017; Chen et al., 2018; Diao et al., 2018). Chen and Zhai (2017) indicated that the active BSISO phases are responsible for the coexisting extremes of precipitation and temperature in

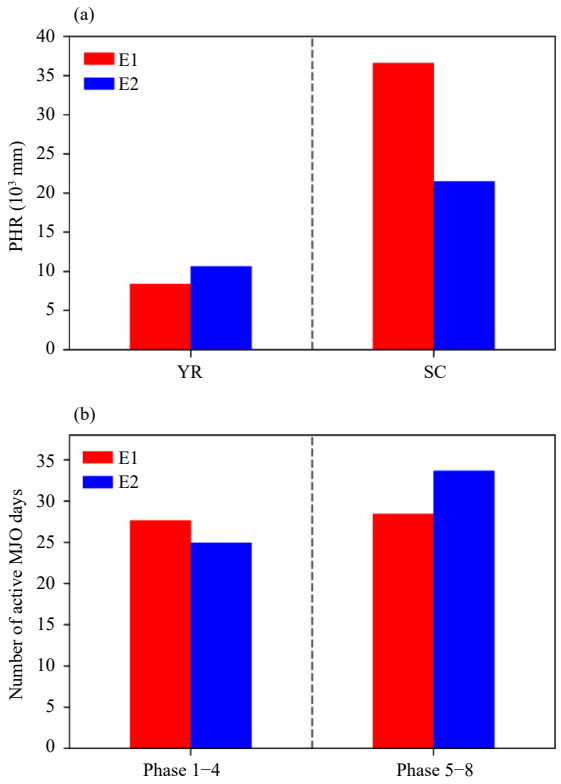

Fig. 16. (a) Area-averaged accumulated wintertime (DJF) PHR amounts (10^3 mm) during E1 (1979–1994, red bars) and E2 (1995–2011, blue bars) relative to the climatology, for the Yangtze River valley (YR) and southeastern China (SC). (b) Same as (a), except for the numbers of active MJO days with amplitude of the Real-time Multivariate MJO (RMM) index greater than 1 for phases 1–4 (two left bars) and phases 5–8 (two right bars).

East Asia. Hsu et al. (2017) and Chen et al. (2018) examined the relative contributions of BSISO1 and BSISO2 to the heatwave events in monsoon Asia. It was found that the occurrence of heatwave in southern China shows a closer relationship with the QBWO (BSISO2) when the QBWO-related anomalous circulations induce an anomalous downward circulation with increased adiabatic heating and solar radiation over southern China. The maintenance and persistence of long-lived heatwave could be attributed to the effects of lower-frequency BSISO1 (Chen et al., 2018). Diao et al. (2018) further showed that the BSISO-related heating anomalies over the tropical monsoon regions can generate anomalous wave train patterns in the middle and higher latitudes, which set up favorable environments for temperature extreme occurrence over the midlatitude North Pacific and the arctic areas.

5. Summary and concluding remarks

In this review paper, we firstly describe from historical perspective the discovery of MJO phenomenon by Chinese scientists. Eight years before the seminal discovery by Madden and Julian (1971), Xie et al. (1963) found a 40–50-day oscillation in zonal wind over five tropical stations including the Canton Island station. Because of their publication in Chinese, the paper did not attract an attention until recently when it was reported in BAMS (Li et al., 2018). In addition to Xie et al. (1963), a number of research works on MJO were published in Chinese in earlier days, including tropical cyclone regulation (Ding et al., 1977) and theoretical understanding of MJO dynamics (Li, 1983, 1985).

The principal causes of the MJO eastward propagation are discussed. For the moisture mode theory, we indicate, for the first time, that there are two types of mechanisms. The first type emphasizes the effect of zonal asymmetry of anomalous moisture in PBL (Hsu and Li, 2012). A positive moisture anomaly induced by PBL convergence in front of convection destabilizes the lower troposphere, promoting the continuous development of shallow, congestus, and deep convection in situ. This promotes eastward propagation of MJO. The second type emphasizes the asymmetry of column integrated MSE tendency, even though the anomalous moisture is symmetric relative to the MJO convection (Sobel and Maloney, 2013). A positive (negative) tendency to the east (west) of the MJO convection, caused by both horizontal and vertical MSE advection, would promote an eastward moving tendency. In the later type, the zonal asymmetry of PBL moisture anomaly is not critical. It is noted that maximum contributions of vertical (horizontal) advection are in the upper (lower) troposphere, while the contribution of horizontal and vertical advection in PBL is small (Wang et al., 2017).

The mechanisms through which MJO convection is initiated over western IO are discussed. It is found that low-level moisture perturbation develops a few days prior to convection initiation over WIO. Such a moisture anomaly is caused by advection of mean moisture by intraseasonal wind associated with the preceding suppressed phase MJO. In addition, upper-tropospheric Rossby wave energy dispersion from Southern Hemispheric midlatitudes may also play a role. A possible scenario through which atmosphere–ocean interactions influence the initiation of MJO is discussed. A cold SSTA generated by a preceding active phase MJO (due to enhanced surface evaporation and reduced downward shortwave radiation) may exert a delayed ocean feedback to initiate a suppressed phase MJO, and vice versa.

MJO exerts a great impact on climate and extreme

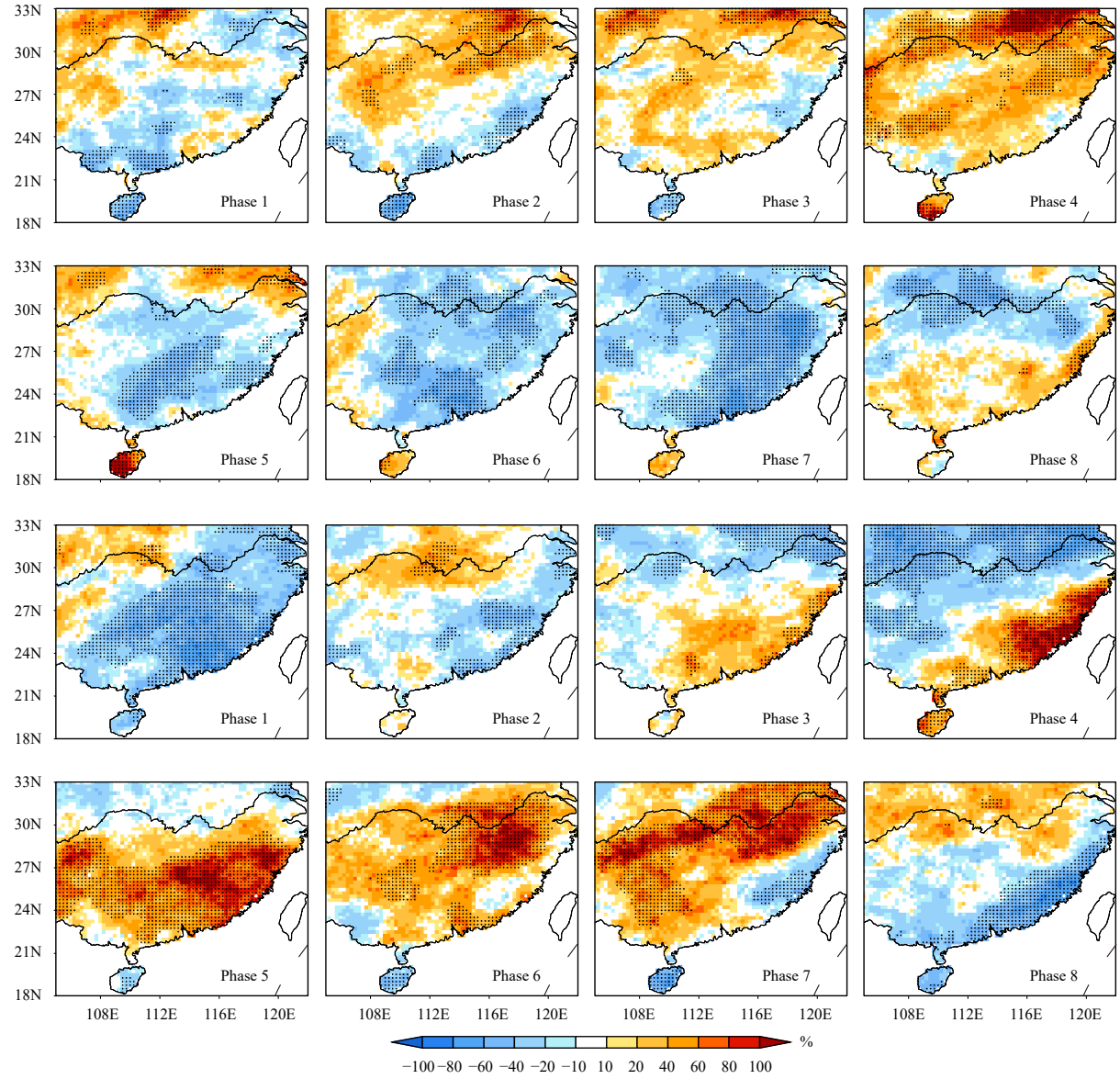

Fig. 17. Percentage change (%) in probability of extreme events at the 90th percentile for each of the 8 phases of BSISO1 (two upper rows) and BSISO2 (two lower rows) with respect to the non-BSISO state. The phases of BSISO are defined according to Lee et al. (2013). The probability of 90th extreme occurrence in a given BSISO phase (P_x) is calculated as the number of days when the rainfall exceeds the 90th percentile divided by the total number of days. Percentage change is computed as $[(P_x - P_{\text{non-BSISO}})/P_{\text{non-BSISO}} \times 100]$, where $P_{\text{non-BSISO}}$ represents the probability of 90th extreme occurrence in the non-BSISO period. Changes exceeding the 95% confidence level are dotted.

weather events over East Asia. The prolonged ice storm event that occurred over South China in January 2008 was resulted from the combined effects of moist/warm southerlies associated with tropical MJO and persistent cold/dry northerlies from high latitudes associated with the Siberian high (Hong and Li, 2009). The MJO modulates the rainfall amount and strength over South China by changing the large-scale circulation pattern and associated moisture transport toward South China (Jia et al., 2011; Liu and Hsu, 2019). When the MJO convections appear over the Indian Ocean, precipitation and extreme rainfall events over the southeastern China are significantly enhanced. In contrast, the precipitation and extreme rainfall events dramatically decrease when the MJO occurs over the western Pacific. During boreal summer, as the BSISO propagates northward into the Asian monsoon area, its anomalous circulations affect the moisture transport and lead to significant changes in rainfall amounts and the probability of rainfall extremes over South China and the Yangtze River basin (Zhang et al., 2009; Hsu et al., 2016). In addition to the influences on monsoon rainfall, the BSISO could also modulate the oc-

currences of heatwave over the Asian monsoon region (Chen and Zhai, 2017; Hsu et al., 2017; Chen et al., 2018) and higher latitudes (e.g., Diao et al., 2018).

Due to limited page number, this review paper is not able to include all MJO related studies. For example, the scale interactions of MJO with high-frequency tropical convectively coupled waves (CCWs) and other climate modes (such as ENSO) have received considerable attention in recent decades. The earlier work of Nakazawa (1988) found that the tropical convections were organized on various spatiotemporal scales, ranging from the short-lived convective cells of a few kilometers to the low-frequency planetary-scale convections, like MJO. Subsequent diagnostic and modeling studies showed that the smaller-scale CCWs (including mixed Rossby–gravity and inertia–gravity waves) within the large-scale MJO envelope and the multi-cloud convective systems (congestus, stratiform, and cumulus clouds) associated with MJO play vital roles in the eastward propagation and maintenance of MJO convection (e.g., Majda and Stechmann, 2009; Khouider et al., 2013; Yang and Ingersoll, 2013, 2014; Zhu et al., 2019). The ENSO–MJO interaction is another important topic. The changes in environmental dynamic and thermodynamic conditions associated with ENSO may exert significant influences on MJO initiation (Hsu and Xiao, 2017), intensity (Deng and Li, 2016; Deng et al., 2016; Wang et al., 2018), propagation (Chen et al., 2016), and periodicity (Liu et al., 2016). The higher-frequency wind associated with MJO, on the other hand, may affect ENSO evolution (e.g., Chen et al., 2017). The multi-scale interaction of MJO is an important topic that is worthy of a more comprehensive review in the future.

Given the importance of MJO activity on global weather and climate systems and its close relevance to extended-range weather prediction, we hope that this paper can serve as a starting point for graduate students and young researchers to know some basics about MJO and to motivate them to read a wider range of literature. Some of the theoretical and modeling results discussed in this paper are not settled yet, and further in-depth studies are needed to challenge the current views so that science can move forward.

REFERENCES

Adames, Á. F., and D. Kim, 2016: The MJO as a dispersive, convectively coupled moisture wave: Theory and observations. *J. Atmos. Sci.*, **73**, 913–941, doi: 10.1175/JAS-D-15-0170.1.

Annamalai, H., and J. M. Slingo, 2001: Active/break cycles: Diagnosis of the intraseasonal variability of the Asian summer monsoon. *Climate Dyn.*, **18**, 85–102, doi: 10.1007/s00382 0100161.

Araligidad, N. M., and E. D. Maloney, 2008: Wind-driven latent heat flux and the intraseasonal oscillation. *Geophys. Res. Lett.*, **35**, L04815, doi: 10.1029/2007GL032746.

Bai, X. X., C. Y. Li, Y. K. Tan, et al., 2011: Analysis of the Madden–Julian Oscillation impacts on the spring rainfall in East China. *J. Trop. Meteor.*, **27**, 814–822, doi: 10.3969/j.issn.1004-4965.2011.06.004. (in Chinese)

Batstone, C. P., A. J. Matthews, and D. P. Stevens, 2005: Coupled ocean–atmosphere interactions between the Madden–Julian oscillation and synoptic-scale variability over the warm pool. *J. Climate*, **18**, 2004–2020, doi: 10.1175/JCLI3398.1.

Cao, X., T. Li, M. Peng, et al., 2014: Effects of monsoon trough interannual variation on tropical cyclogenesis over the western North Pacific. *Geophys. Res. Lett.*, **41**, 4332–4339, doi: 10.1002/2014GL060307.

Chang, C. P., and H. Lim, 1988: Kelvin wave-CISK: A possible mechanism for the 30–50 day oscillations. *J. Atmos. Sci.*, **45**, 1709–1720, doi: 10.1175/1520-0469(1988)045<1709:KW-CAPM>2.0.CO;2.

Chang, M.-Y., T. Li, P.-L. Lin, et al., 2019: Forecasts of MJO events during DYNAMO with a coupled atmosphere–ocean model: Sensitivity to cumulus parameterization scheme. *J. Meteor. Res.*, **33**, 1016–1030, doi: 10.1007/s13351-019-9062-5.

Chen, L., T. Li, B. Wang, et al., 2017: Formation mechanism for 2015/16 super El Niño. *Sci. Rep.*, **7**, 2975, doi: 10.1038/s41598-017-02926-3.

Chen, R. D., Z. P. Wen, and R. Y. Lu, 2018: Large-scale circulation anomalies and intraseasonal oscillations associated with long-lived extreme heat events in South China. *J. Climate*, **31**, 213–232, doi: 10.1175/JCLI-D-17-0232.1.

Chen, T. C., and M. Murakami, 1988: The 30–50 day variation of convective activity over the western Pacific Ocean with emphasis on the northwestern region. *Mon. Wea. Rev.*, **116**, 892–906, doi: 10.1175/1520-0493(1988)116<0892:TDVOCA>2.0.CO;2.

Chen, X., J. Ling, and C. Y. Li, 2016: Evolution of the Madden–Julian oscillation in two types of El Niño. *J. Climate*, **29**, 1919–1934, doi: 10.1175/JCLI-D-15-0486.1.

Chen, Y., and P. M. Zhai, 2017: Simultaneous modulations of precipitation and temperature extremes in southern parts of China by the boreal summer intraseasonal oscillation. *Climate Dyn.*, **49**, 3363–3381, doi: 10.1007/s00382-016-3518-4.

Deng, L., and T. Li, 2016: Relative roles of background moisture and vertical shear in regulating interannual variability of boreal summer intraseasonal oscillations. *J. Climate*, **29**, 7009–7025, doi: 10.1175/JCLI-D-15-0498.1.

Deng, L., T. Li, J. Liu, et al., 2016: Factors controlling the interannual variations of MJO intensity. *J. Meteor. Res.*, **30**, 328–340, doi: 10.1007/s13351-016-5113-3.

Diao, Y. F., T. Li, and P.-C. Hsu, 2018: Influence of the boreal summer intraseasonal oscillation on extreme temperature events in the Northern Hemisphere. *J. Meteor. Res.*, **32**, 534–547, doi: 10.1007/s13351-018-8031-8.

Ding, Y. H., H. J. Feng, Q. F. Xue, et al., 1977: A preliminary study on the simultaneous developments of the multiple typhoons in the intertropical convergence zone. *Chinese J. Atmos. Sci.*, **1**, 89–98, doi: 10.3878/j.issn.1006-9895.1977.02.02. (in Chinese)

Emanuel, K. A., 1987: An air–sea interaction model of intraseasonal oscillations in the tropics. *J. Atmos. Sci.*, **44**, 2324–2340, doi:10.1175/1520-0469(1987)044<2324:AASIMO>2.0.CO;2.

Gill, A. E., 1980: Some simple solutions for heat-induced tropical circulation. *Quart. J. Roy. Meteor. Soc.*, **106**, 447–462, doi: 10.1002/qj.49710644905.

Hartmann, D. L., and M. L. Michelsen, 1989: Intraseasonal periodicities in Indian rainfall. *J. Atmos. Sci.*, **46**, 2838–2862, doi: 10.1175/1520-0469(1989)046<2838:IPIIR>2.0.CO;2.

Hartmann, D. L., and E. D. Maloney, 2001: The Madden–Julian oscillation, barotropic dynamics, and North Pacific tropical cyclone formation. Part II: Stochastic barotropic modeling. *J. Atmos. Sci.*, **58**, 2559–2570, doi: 10.1175/1520-0469(2001)058<2559:TMJOBD>2.0.CO;2.

Hendon, H. H., and B. Liebmann, 1994: Organization of convection within the Madden–Julian oscillation. *J. Geophys. Res. Atmos.*, **99**, 8073–8083, doi: 10.1029/94JD00045.

Hendon, H. H., and M. L. Salby, 1994: The life cycle of the Madden–Julian Oscillation. *J. Atmos. Sci.*, **51**, 2225–2237, doi: 10.1175/1520-0469(1994)051<2225:TLCOTM>2.0.CO;2.

Hong, C. C., and T. Li, 2009: The extreme cold anomaly over southeast Asia in February 2008: Roles of ISO and ENSO. *J. Climate*, **22**, 3786–3801, doi: 10.1175/2009JCLI2864.1.

Hsu, H. H., and C. H. Weng, 2001: Northwestward propagation of the intraseasonal oscillation in the western North Pacific during the boreal summer: Structure and mechanism. *J. Climate*, **14**, 3834–3850, doi: 10.1175/1520-0442(2001)014<3834:NPOTIO>2.0.CO;2.

Hsu, H. H., B. J. Hoskins, and F. F. Jin, 1990: The 1985/86 intraseasonal oscillation and the role of the extratropics. *J. Atmos. Sci.*, **47**, 823–839, doi: 10.1175/1520-0469(1990)047<0823:TIOATR>2.0.CO;2.

Hsu, P. C., and T. Li, 2011: Interactions between boreal summer intraseasonal oscillations and synoptic-scale disturbances over the western North Pacific. Part II: Apparent heat and moisture sources and eddy momentum transport. *J. Climate*, **24**, 942–961, doi: 10.1175/2010JCLI3834.1.

Hsu, P. C., and T. Li, 2012: Role of the boundary layer moisture asymmetry in causing the eastward propagation of the Madden–Julian Oscillation. *J. Climate*, **25**, 4914–4931, doi: 10.1175/JCLI-D-11-00310.1.

Hsu, P. C., and Y. Yang, 2016: Contribution of atmospheric internal processes to the interannual variability of the South Asian summer monsoon. *Int. J. Climatol.*, **36**, 2917–2930, doi: 10.1002/joc.4528.

Hsu, P. C., and T. Xiao, 2017: Differences in the initiation and development of the Madden–Julian Oscillation over the Indian Ocean associated with two types of El Niño. *J. Climate*, **30**, 1397–1415, doi: 10.1175/JCLI-D-16-0336.1.

Hsu, P. C., T. Li, and C. H. Tsou, 2011: Interactions between boreal summer intraseasonal oscillations and synoptic-scale disturbances over the western North Pacific. Part I: Energetics diagnosis. *J. Climate*, **24**, 927–941, doi: 10.1175/2010JCLI3833.1.

Hsu, P. C., T. Li, and H. Murakami, 2014: Moisture asymmetry and MJO eastward propagation in an aquaplanet general circulation model. *J. Climate*, **27**, 8747–8760, doi: 10.1175/JCLI-D-14-00148.1.

Hsu, P. C., J.-Y. Lee, and K.-J. Ha, 2016: Influence of boreal summer intraseasonal oscillation on rainfall extremes in southern China. *Int. J. Climatol.*, **36**, 1403–1412, doi: 10.1002/joc.4433.

Hsu, P. C., J.-Y. Lee, K.-J. Ha, et al., 2017: Influences of boreal summer intraseasonal oscillation on heat waves in monsoon Asia. *J. Climate*, **30**, 7191–7211, doi: 10.1175/JCLI-D-16-0505.1.

Jia, X., L. J. Chen, F. M. Ren, et al., 2011: Impacts of the MJO on winter rainfall and circulation in China. *Adv. Atmos. Sci.*, **28**, 521–533, doi: 10.1007/s00376-010-9118-z.

Jiang, X. A., and T. Li, 2005: Reinitiation of the boreal summer intraseasonal oscillation in the tropical Indian Ocean. *J. Climate*, **18**, 3777–3795, doi: 10.1175/JCLI3516.1.

Jiang, X. A., D. E. Waliser, P. K. Xavier, et al., 2015: Vertical structure and physical processes of the Madden–Julian oscillation: Exploring key model physics in climate simulations. *J. Geophys. Res. Atmos.*, **120**, 4718–4748, doi: 10.1002/2014JD022375.

Jiang, X. A., T. Li, and B. Wang, 2004: Structures and mechanisms of the northward propagating boreal summer intraseasonal oscillation. *J. Climate*, **17**, 1022–1039, doi: 10.1175/1520-0442(2004)017<1022:SAMOTN>2.0.CO;2.

Jones, C., and B. C. Weare, 1996: The role of low-level moisture convergence and ocean latent heat fluxes in the Madden and Julian Oscillation: An observational analysis using ISCCP data and ECMWF analyses. *J. Climate*, **9**, 3086–3104, doi: 10.1175/1520-0442(1996)009<3086:TROLLM>2.0.CO;2.

Jones, C., L. M. V. Carvalho, R. Wayne Higgins, et al., 2004: Climatology of tropical intraseasonal convective anomalies: 1979–2002. *J. Climate*, **17**, 523–539, doi: 10.1175/1520-0442(2004)017<0523:COTICA>2.0.CO;2.

Khouider, B., A. J. Majda, and S. N. Stechmann, 2013: Climate science in the tropics: Waves, vortices and PDEs. *Nonlinearity*, **26**, R1, doi: 10.1088/0951-7715/26/1/R1.

Kikuchi, K., B. Wang, and Y. Kajikawa, 2012: Bimodal representation of the tropical intraseasonal oscillation. *Climate Dyn.*, **38**, 1989–2000, doi: 10.1007/s00382-011-1159-1.

Kiladis, G. N., K. H. Straub, and P. T. Haertel, 2005: Zonal and vertical structure of the Madden–Julian Oscillation. *J. Atmos. Sci.*, **62**, 2790–2809, doi: 10.1175/JAS3520.1.

Kim, D., J. S. Kug, and A. H. Sobel, 2014: Propagating versus nonpropagating Madden–Julian Oscillation events. *J. Climate*, **27**, 111–125, doi: 10.1175/JCLI-D-13-00084.1.

Knutson, T. R., and K. M. Weickmann, 1987: 30–60 day atmospheric oscillations: Composite life cycles of convection and circulation anomalies. *Mon. Wea. Rev.*, **115**, 1407–1436, doi: 10.1175/1520-0493(1987)115<1407:DAOCLC>2.0.CO;2.

Krishnamurti, T. N., and D. Subrahmanyam, 1982: The 30–50 day mode at 850 mb during MONEX. *J. Atmos. Sci.*, **39**, 2088–2095, doi: 10.1175/1520-0469(1982)039<2088:TDMAMD>2.0.CO;2.

Lau, K., and P. H. Chan, 1986: Aspects of the 40–50 day oscillation during the northern summer as inferred from outgoing longwave radiation. *Mon. Wea. Rev.*, **114**, 1354–1367, doi: 10.1175/1520-0493(1986)114<1354:AOTDOD>2.0.CO;2.

Lau, K. H., and N. C. Lau, 1990: Observed structure and propagation characteristics of tropical summertime synoptic scale disturbances. *Mon. Wea. Rev.*, **118**, 1888–1913, doi: 10.1175/1520-0493(1990)118<1888:OSAPCO>2.0.CO;2.

Lau, K. M., and L. Peng, 1987: Origin of low-frequency (intraseasonal) oscillations in the tropical atmosphere. Part I: Basic theory. *J. Atmos. Sci.*, **44**, 950–972, doi: 10.1175/1520-0469(1987)044<0950:OOLFOI>2.0.CO;2.

Lawrence, D. M., and P. J. Webster, 2002: The boreal summer intraseasonal oscillation: Relationship between northward and eastward movement of convection. *J. Atmos. Sci.*, **59**, 1593–1606, doi: 10.1175/1520-0469(2002)059<1593:TBSIOR>2.0.CO;2.

Lee, J. Y., B. Wang, M. C. Wheeler, et al., 2013: Real-time multivariate indices for the boreal summer intraseasonal oscillation over the Asian summer monsoon region. *Climate Dyn.*, **40**, 493–509, doi: 10.1007/s00382-012-1544-4.

Lengaigne, M., E. Guilyardi, J. P. Boulanger, et al., 2004: Triggering of El Niño by westerly wind events in a coupled general circulation model. *Climate Dyn.*, **23**, 601–620, doi: 10.1007/s00382-004-0457-2.

Li, C. Y., 1983: Convective condensation heating and unstable mode. *Chinese J. Atmos. Sci.*, **7**, 260–268, doi: 10.3878/j.issn.1006-9895.1983.03.03. (in Chinese)

Li, C. Y., 1985: Actions of summer monsoon troughs (ridges) and tropical cyclone over South Asia and the moving CISK mode. *Sci. in China Ser. B*, **28**, 1197–1206.

Li, C. Y., H.-R. Cho, and J.-T. Wang, 2002: CISK Kelvin wave with evaporation–wind feedback and air–sea interaction—A further study of tropical intraseasonal oscillation mechanism. *Adv. Atmos. Sci.*, **19**, 379–390, doi: 10.1007/s00376-002-0073-1.

Li, C. Y., X. L. Jia, J. Ling, et al., 2009: Sensitivity of MJO simulations to diabatic heating profiles. *Climate Dyn.*, **32**, 167–187, doi: 10.1007/s00382-008-0455-x.

Li, K. P., W. D. Yu, T. Li, et al., 2013: Structures and mechanisms of the first-branch northward-propagating intraseasonal oscillation over the tropical Indian Ocean. *Climate Dyn.*, **40**, 1707–1720, doi: 10.1007/s00382-012-1492-z.

Li, T., 2014: Recent advance in understanding the dynamics of the Madden–Julian oscillation. *J. Meteor. Res.*, **28**, 1–33, doi: 10.1007/s13351-014-3087-6.

Li, T., and B. Wang, 1994: The influence of sea surface temperature on the tropical intraseasonal oscillation: A numerical study. *Mon. Wea. Rev.*, **122**, 2349–2362, doi: 10.1175/1520-0493(1994)122<2349:TIOSST>2.0.CO;2.

Li, T., and B. Wang, 2005: A review on the western North Pacific monsoon: Synoptic-to-interannual variabilities. *Terrestrial, Atmospheric and Oceanic Sciences*, **16**, 285–314, doi: 10.3319/TAO.2005.16.2.285(A).

Li, T., and C. H. Zhou, 2009: Planetary scale selection of the Madden–Julian Oscillation. *J. Atmos. Sci.*, **66**, 2429–2443, doi: 10.1175/2009JAS2968.1.

Li, T., and F. Hu, 2019: A coupled moisture–dynamics model of the Madden–Julian oscillation: Convection interaction with first and second baroclinic modes and planetary boundary layer. *Climate Dyn.*, **53**, 5529–5546, doi: 10.1007/s00382-019-04879-x.

Li, T., F. Tam, X. Fu, et al., 2008: Causes of the intraseasonal SST variability in the tropical Indian Ocean. *Atmos. Ocean. Sci. Lett.*, **1**, 18–23, doi: 10.1080/16742834.2008.11446758.

Li, T., C. B. Zhao, P. C. Hsu, et al., 2015: MJO initiation processes over the tropical Indian Ocean during DYNAMO/CINDY2011. *J. Climate*, **28**, 2121–2135, doi: 10.1175/JCLI-D-14-00328.1.

Li, T., L. Wang, M. Peng, et al., 2018: A paper on the tropical intraseasonal oscillation published in 1963 in a Chinese journal. *Bull. Amer. Meteor. Soc.*, **99**, 1765–1779, doi: 10.1175/BAMS-D-17-0216.1.

Liebmann, B., H. H. Hendon, and J. D. Glick, 1994: The relationship between tropical cyclones of the western Pacific and Indian Oceans and the Madden–Julian oscillation. *J. Meteor. Soc. Japan*, **72**, 401–412, doi: 10.2151/jmsj1965.72.3_401.

Lindzen, R. S., and S. Nigam, 1987: On the role of sea surface temperature gradients in forcing low-level winds and convergence in the tropics. *J. Atmos. Sci.*, **44**, 2418–2436, doi: 10.1175/1520-0469(1987)044<2418:OTROSS>2.0.CO;2.

Liu, F., T. Li, H. Wang, et al., 2016: Modulation of boreal summer intraseasonal oscillations over the western North Pacific by ENSO. *J. Climate*, **29**, 7189–7201, doi: 10.1175/JCLI-D-15-0831.1.

Liu, H. B., J. Yang, D. L. Zhang, et al., 2014: Roles of synoptic to quasi-biweekly disturbances in generating the summer 2003 heavy rainfall in East China. *Mon. Wea. Rev.*, **142**, 886–904, doi: 10.1175/MWR-D-13-00055.1.

Liu, Y., and P. C. Hsu, 2019: Long-term changes in wintertime persistent heavy rainfall over southern China contributed by the Madden–Julian Oscillation. *Atmos. Ocean. Sci. Lett.*, **12**, 361–368, doi: 10.1080/16742834.2019.1639471.

Lu, J. H., T. Li, and L. Wang, 2019: Precipitation diurnal cycle over the Maritime Continent modulated by the MJO. *Climate Dyn.*, **53**, 6489–6501, doi: 10.1007/s00382-019-04941-8.

Lu, W., and P. C. Hsu, 2017: Factors controlling the seasonality of the Madden–Julian Oscillation. *Dyn. Atmos. Oceans*, **78**, 106–120, doi: 10.1016/j.dynatmoce.2017.04.002.

Madden, R. A., 1986: Seasonal variations of the 40–50 day oscillation in the tropics. *J. Atmos. Sci.*, **43**, 3138–3158, doi: 10.1175/1520-0469(1986)043<3138:SVOTDO>2.0.CO;2.

Madden, R. A., and P. R. Julian, 1971: Detection of a 40–50 day oscillation in the zonal wind in the tropical Pacific. *J. Atmos. Sci.*, **28**, 702–708, doi: 10.1175/1520-0469(1971)028<0702:DOADOI>2.0.CO;2.

Madden, R. A., and P. R. Julian, 1972: Description of global-scale circulation cells in the tropics with a 40–50 day period. *J. Atmos. Sci.*, **29**, 1109–1123, doi: 10.1175/1520-0469(1972)029<1109:DOGSCC>2.0.CO;2.

Madden, R. A., and P. R. Julian, 1994: Observations of the 40–50-day tropical oscillation—A review. *Mon. Wea. Rev.*, **122**, 814–837, doi: 10.1175/1520-0493(1994)122<0814:OOTDTO>2.0.CO;2.

Majda, A. J., and S. N. Stechmann, 2009: The skeleton of tropical intraseasonal oscillations. *Proc. Natl. Acad. Sci. USA*, **106**, 8417–8422, doi: 10.1073/pnas.0903367106.

Maloney, E. D., and D. L. Hartmann, 1998: Frictional moisture convergence in a composite life cycle of the Madden–Julian oscillation. *J. Climate*, **11**, 2387–2403, doi: 10.1175/1520-0442(1998)011<2387:FMCIAC>2.0.CO;2.

Maloney, E. D., and D. L., Hartmann, 2000a: Modulation of eastern North Pacific hurricanes by the Madden–Julian oscillation. *J. Climate*, **13**, 1451–1460, doi: 10.1175/1520-0442(2000)013<1451:MOENPH>2.0.CO;2.

Maloney, E. D., and D. L., Hartmann, 2000b: Modulation of hur-

ricane activity in the Gulf of Mexico by the Madden–Julian oscillation. *Science*, **287**, 2002–2004, doi: 10.1126/science.287.5460.2002.

Maloney, E. D., and D. L. Hartmann, 2001: The Madden–Julian oscillation, barotropic dynamics, and North Pacific tropical cyclone formation. Part I: Observations. *J. Atmos. Sci.*, **58**, 2545–2558, doi: 10.1175/1520-0469(2001)058<2545:TMJOBD>2.0.CO;2.

Maloney, E. D., and M. J. Dickinson, 2003: The intraseasonal oscillation and the energetics of summertime tropical western North Pacific synoptic-scale disturbances. *J. Atmos. Sci.*, **60**, 2153–2168, doi: 10.1175/1520-0469(2003)060<2153:TIOATE>2.0.CO;2.

Mao, J. Y., Z. Sun, and G.-X. Wu, 2010: 20–50-day oscillation of summer Yangtze rainfall in response to intraseasonal variations in the subtropical high over the western North Pacific and South China Sea. *Climate Dyn.*, **34**, 747–761, doi: 10.1007/s00382-009-0628-2.

Matthews, A. J., 2000: Propagation mechanisms for the Madden–Julian Oscillation. *Quart. J. Roy. Meteor. Soc.*, **126**, 2637–2651, doi: 10.1002/qj.49712656902.

Matthews, A. J., 2008: Primary and successive events in the Madden–Julian oscillation. *Quart. J. Roy. Meteor. Soc.*, **134**, 439–453, doi: 10.1002/qj.224.

Murakami, T., and T. Nakazawa, 1985: Tropical 45 day oscillations during the 1979 Northern Hemisphere summer. *J. Atmos. Sci.*, **42**, 1107–1122, doi: 10.1175/1520-0469(1985)042<1107:TDODTN>2.0.CO;2.

Nakazawa, T., 1988: Tropical super clusters within intraseasonal variations over the western Pacific. *J. Meteor. Soc. Japan*, **66**, 823–839, doi: 10.2151/jmsj1965.66.6_823.

Neelin, J. D., and I. M. Held, 1987: Modeling tropical convergence based on the moist static energy budget. *Mon. Wea. Rev.*, **115**, 3–12, doi: 10.1175/1520-0493(1987)115<0003:MTCBOT>2.0.CO;2.

Neelin, J. D., I. M. Held, and K. H. Cook, 1987: Evaporation–wind feedback and low-frequency variability in the tropical atmosphere. *J. Atmos. Sci.*, **44**, 2341–2348, doi: 10.1175/1520-0469(1987)044<2341:EWFALF>2.0.CO;2.

Qi, Y. J., R. H. Zhang, T. Li, et al., 2008: Interactions between the summer mean monsoon and the intraseasonal oscillation in the Indian monsoon region. *Geophys. Res. Lett.*, **35**, L17704, doi: 10.1029/2008GL034517.

Salby, M. L., and H. H. Hendon, 1994: Intraseasonal behavior of clouds, temperature, and motion in the tropics. *J. Atmos. Sci.*, **51**, 2207–2224, doi: 10.1175/1520-0469(1994)051<2207:IBOCTA>2.0.CO;2.

Seo, K. H., and K. Y. Kim, 2003: Propagation and initiation mechanisms of the Madden–Julian oscillation. *J. Geophys. Res. Atmos.*, **108**, 4384, doi: 10.1029/2002JD002876.

Shinoda, T., H. H. Hendon, and J. Glick, 1998: Intraseasonal variability of surface fluxes and sea surface temperature in the tropical western Pacific and Indian Oceans. *J. Climate*, **11**, 1685–1702, doi: 10.1175/1520-0442(1998)011<1685:IVOSFA>2.0.CO;2.

Sobel, A., and E. Maloney, 2012: An idealized semi-empirical framework for modeling the Madden–Julian oscillation. *J. Atmos. Sci.*, **69**, 1691–1705, doi: 10.1175/JAS-D-11-0118.1.

Sobel, A., and E. Maloney, 2013: Moisture modes and the eastward propagation of the MJO. *J. Atmos. Sci.*, **70**, 187–192, doi: 10.1175/JAS-D-12-0189.1.

Sperber, K. R., 2003: Propagation and the vertical structure of the Madden–Julian oscillation. *Mon. Wea. Rev.*, **131**, 3018–3037, doi: 10.1175/1520-0493(2003)131<3018:PATVSO>2.0.CO;2.

Sperber, K. R., J. M. Slingo, P. M. Inness, et al., 1997: On the maintenance and initiation of the intraseasonal oscillation in the NCEP/NCAR reanalysis and in the GLA and UKMO AMIP simulations. *Climate Dyn.*, **13**, 769–795, doi: 10.1007/s003820050197.

Straub, K. H., and G. N. Kiladis, 2003: Interactions between the boreal summer intraseasonal oscillation and higher-frequency tropical wave activity. *Mon. Wea. Rev.*, **131**, 945–960, doi: 10.1175/1520-0493(2003)131<0945:IBTBSI>2.0.CO;2.

Tsou, C. H., P. C. Hsu, W. S. Kau, et al., 2005: Northward and northwestward propagation of 30–60 day oscillation in the tropical and extratropical western North Pacific. *J. Meteor. Soc. Japan*, **83**, 711–726, doi: 10.2151/jmsj.83.711.

Waliser, D. E., 2006: Intraseasonal variability. *The Asian Monsoon*, B. Wang, Ed., Springer, Berlin, Heidelberg, 203–257, doi: 10.1007/3-540-37722-0_5.

Wang, B., 1988a: Dynamics of tropical low-frequency waves: An analysis of the moist Kelvin wave. *J. Atmos. Sci.*, **45**, 2051–2065, doi: 10.1175/1520-0469(1988)045<2051:DOTLFW>2.0.CO;2.

Wang, B., 1988b: Comments on "An air–sea interaction model of intraseasonal oscillation in the tropics". *J. Atmos. Sci.*, **45**, 3521–3525, doi: 10.1175/1520-0469(1988)045<3521:COAIMO>2.0.CO;2.

Wang, B., and H. Rui, 1990: Synoptic climatology of transient tropical intraseasonal convection anomalies: 1975–1985. *Meteor. Atmos. Phys.*, **44**, 43–61, doi: 10.1007/BF01026810.

Wang, B., and T. M. Li, 1993: A simple tropical atmosphere model of relevance to short-term climate variations. *J. Atmos. Sci.*, **50**, 260–284, doi: 10.1175/1520-0469(1993)050<0260:ASTAMO>2.0.CO;2.

Wang, B., and T. M. Li, 1994: Convective interaction with boundary-layer dynamics in the development of a tropical intraseasonal system. *J. Atmos. Sci.*, **51**, 1386–1400, doi: 10.1175/1520-0469(1994)051<1386:CIWBLD>2.0.CO;2.

Wang, B., P. Webster, K. Kikuchi, et al., 2006: Boreal summer quasi-monthly oscillation in the global tropics. *Climate Dyn.*, **27**, 661–675, doi: 10.1007/s00382-006-0163-3.

Wang, L., T. Li, L. Chen, et al., 2018: Modulation of the MJO intensity over the equatorial western Pacific by two types of El Niño. *Climate Dyn.*, **51**, 687–700, doi: 10.1007/s00382-017-3949-6.

Wang, L., T. Li, E. Maloney, et al., 2017: Fundamental causes of propagating and nonpropagating MJOs in MJOTF/GASS models. *J. Climate*, **30**, 3743–3769, doi: 10.1175/JCLI-D-16-0765.1.

Weickmann, K. M., 1983: Intraseasonal circulation and outgoing longwave radiation modes during Northern Hemisphere winter. *Mon. Wea. Rev.*, **111**, 1838–1858, doi: 10.1175/1520-0493(1983)111<1838:ICAOLR>2.0.CO;2.

Xie, Y. B., S. J. Chen, Y. L. Zhang, et al., 1963: A preliminarily statistic and synoptic study about the basic currents over southeastern Asia and the initiation of typhoons. *Acta Meteor. Sinica*, **33**, 206–217, doi: 10.11676/qxxb1963.020. (in

Chinese)

Yang, D., and A. P. Ingersoll, 2013: Triggered convection, gravity waves, and the MJO: A shallow-water model. *J. Atmos. Sci.*, **70**, 2476–2486, doi: 10.1175/JAS-D-12-0255.1.

Yang, D., and A. P. Ingersoll, 2014: A theory of the MJO horizontal scale. *Geophys. Res. Lett.*, **41**, 1059–1064, doi: 10.1002/2013GL058542.

Yang, H., and C. Y. Li, 2003: The relation between atmospheric intraseasonal oscillation and summer severe flood and drought in the Changjiang–Huaihe River Basin. *Adv. Atmos. Sci.*, **20**, 540–553, doi: 10.1007/BF02915497.

Yao, Y. H., H. Lin, and Q. Q. Wu, 2015: Subseasonal variability of precipitation in China during boreal winter. *J. Climate*, **28**, 6548–6559, doi: 10.1175/JCLI-D-15-0033.1.

Yasunari, T., 1979: Cloudiness fluctuations associated with the Northern Hemisphere summer monsoon. *J. Meteor. Soc. Japan*, **57**, 227–242, doi: 10.2151/jmsj1965.57.3_227.

Yasunari, T., 1980: A quasi-stationary appearance of 30 to 40 day period in the cloudiness fluctuation during the summer monsoon over India. *J. Meteor. Soc. Japan*, **58**, 225–229, doi: 10.2151/jmsj1965.58.3_225.

Zhang, C. D., 2005: Madden–Julian oscillation. *Rev. Geophys.*, **43**, G2003, doi: 10.1029/2004RG000158.

Zhang, C. D., and M. Dong, 2004: Seasonality in the Madden–Julian oscillation. *J. Climate*, **17**, 3169–3180, doi: 10.1175/1520-0442(2004)017<3169:SITMO>2.0.CO;2.

Zhang, L. N., B. Z. Wang, and Q. C. Zeng, 2009: Impact of the Madden–Julian Oscillation on summer rainfall in Southeast China. *J. Climate*, **22**, 201–216, doi: 10.1175/2008JCLI1959.1.

Zhang, Q. C., T. Li, and J. Liu, 2019: Contrast of evolution characteristics of boreal summer and winter intraseasonal oscillations over tropical Indian Ocean. *J. Meteor. Res.*, **33**, 678–694, doi: 10.1007/s13351-019-9015-z.

Zhao, C., and T. Li, 2019: Basin dependence of the MJO modulating tropical cyclone genesis. *Climate Dyn.*, **52**, 6081–6096, doi: 10.1007/s00382-018-4502-y.

Zhao, C. B., T. Li, and T. J. Zhou, 2013: Precursor signals and processes associated with MJO initiation over the tropical Indian Ocean. *J. Climate*, **26**, 291–307, doi: 10.1175/JCLI-D-12-00113.1.

Zhou, C. H., and T. Li, 2010: Upscale feedback of tropical synoptic variability to intraseasonal oscillations through the nonlinear rectification of the surface latent heat flux. *J. Climate*, **23**, 5738–5754, doi: 10.1175/2010JCLI3468.1.

Zhu, C. W., T. Nakazawa, J. P. Li, et al., 2003: The 30–60 day intraseasonal oscillation over the western North Pacific Ocean and its impacts on summer flooding in China during 1998. *Geophys. Res. Lett.*, **30**, 1952, doi: 10.1029/2003GL017817.

Zhu, Y., T. Li, M. Zhao, et al., 2019: Interaction between the MJO and high-frequency waves over the Maritime Continent in boreal winter. *J. Climate*, **32**, 3819–3835, doi: 10.1175/JCLI-D-18-0511.1.

Tech & Copy Editor: Lan YI